Acta Geotechnica (2021) 16:1205–1230
https://doi.org/10.1007/s11440-020-01069-6

RESEARCH PAPER

Laboratory investigation of pullout behavior of hollow and solid shaft helical nail in frictional soil

Pankaj Sharma[1] · Saurabh Rawat[1] · Ashok Kumar Gupta[1]

Received: 24 October 2019 / Accepted: 20 July 2020 / Published online: 25 September 2020

Abstract
Helical soil nails are passive elements installed in the soil which attains its bond strength through skin friction and bearing from helices. The present study examines the behavior of helical soil nail installed in cohesionless soil subjected to pullout force under varying parameters such as helical nail configuration (shaft diameter, helical diameter, helical pitch, number of helices), nail shaft types (roughness and stiffness), installation torque, and overburden pressure. The installation torque and corresponding nail pullout capacity can be established using a torque correlation factor (K_t). K_t value decreases with increasing embedded nail area and is inversely proportional to the nail shaft diameter. From pullout tests result, it is found that pitch in the range of 24.5–35.5 mm shows better pullout capacity. Also, results show that additional helices will only contribute to pullout capacity if located outside the region of soil mobilized in the failure mechanism of lower helix. Moreover, higher axial strains are found for hollow shaft nail, which alters with the increase in number of helices. Test results also indicate that various hollow shaft helical nails have nearly equal interaction friction angle to solid shaft helical soil nails with lesser shaft diameter. Therefore, it is concluded that solid shaft helical nails can be replaced by hollow nails without compromising on pullout capacity adding to reduction in construction cost. Tests results show linear correlation between maximum pullout shear stress and overburden pressure following a Mohr–Coulomb failure for different helical nail types.

Keywords Helical soil nail · Hollow and solid shaft · Interaction factor · Pullout capacity · Torque correlation factor

1 Introduction

Conventional soil nailing technique of drilling boreholes and placing a passive element along with cement grout has been widely used for stabilizing excavations, tunnels, slopes, and highway embankments [4]. However, during installation of conventional soil nails, drilling and grouting operation causes disturbance to the in situ soil properties. During bore hole drilling, soil settles down and causes local slope failure. Similarly, due to grouting pressure, loose soil undergoes fracturing which hampers the soil–nail and soil–soil interactive bonding. In order to overcome the difficulties associated with conventional soil nailing technique, researchers have attempted to develop passive elements which can mobilize better interaction with surrounding soil and provide subsequent reinforcement against failure. In view of this, development of groutless spiral nails [1] and self-drilled soil nails [17] has been undertaken. Realizing the basic concept of driving maximum interaction from surrounding soil without excessively disturbing the in situ stress condition, few researchers [23, 26, 30, 31, 34] tried to use the concept of helical piles and helical anchors for amending the conventional soil nail installation issues by use of a novel soil nail called helical soil nail. A helical soil nail consists of a shaft (circular or square) with helical plates attached along the nail length at regular spacing. However, the basic difference between a helical pile and anchor to that with helical soil nail lies within the stresses mobilized around the nail. Uniform stresses are developed

✉ Pankaj Sharma
iisc0700ps@gmail.com

✉ Saurabh Rawat
saurabh.rawat@juit.ac.in

Ashok Kumar Gupta
ashok.gupta@juit.ac.in

[1] Department of Civil Engineering, Jaypee University of Information Technology, Solan, HP 173234, India

during failure in cases of helical pile/anchor [9], whereas stresses around the helical soil nail are found to be non–uniform. Moreover, the bearing from helical plates in helical soil nails acts against the horizontal stresses instead of vertical stresses as found during pullout studies conducted on helical piles and helical anchors. Although the pullout mechanism of helical pile/anchors is found to be different, it was realized that utilization of additional bearing from helical plates can be beneficial in reducing the installation difficulties of conventional soil nails. Simultaneously, bearing along with shaft friction will not only reduce drilling and grouting labor but also enhance soil–nail interaction. Another advantage of helical soil nailing can be realized with the fact that in the absence of drilling and grouting requirement, helical soil nailing can be conducted even in areas with high water table. Moreover, problematic soil condition such as loose clean granular sand or soils with excessive moisture or wet pockets which are unable to withstand prior to nail installation can also be rectified. Due to rotating mechanism (torque) during installation of helical nails, less vibration will be produced in the surrounding soil as compared to drilling and grouting. Moreover, negligible spoil generation will induce almost null shipping or dumping cost rendering construction of helical nails structures as economical.

During displacement of helical soil-nailed structure under loading condition, the following four forces are mobilized in helical nail, namely i) tension forces, ii) pullout resistance, iii) skin friction, and iv) bearing resistance. The study of reported literature [8, 9, 13, 32, 39] reveals that pullout resistance is the second most important parameter that governs nail force mobilization during failure after tensile strength of nail. The interface shear strength of conventional soil nail has been investigated through laboratory pullout tests and numerical modeling by various researchers [5, 32, 36, 37, 39]. However, laboratory and numerical studies on pullout studies on helical soil nails are still limited [24–26, 30, 34] with Sharma et al. [30] being the only reported literature regarding installation torque for helical soil nails. The authors have conducted a limited study covering only the variation of installation torque with embedded length and number of helices. The study suggested that installation torque varies linearly with embedded length. Moreover, helical soil nail with double helices requires larger installation torque and consequently renders more pullout capacity. Thus, a lacuna is found for in-depth comprehension of helical soil nail behavior during torque installation and pullout. Nevertheless, development of various torque factors for parametric variations such as pullout capacity, shaft diameter, shaft roughness, number of helices, overburden, helical pitch, and embedded helical nail length encapsulated the novelty of the present study. To investigate the above-stated rationales, a sequence of pullout tests is conducted using a pullout testing machine exclusively designed for helical soil nails for optimizing of different helical soil nail configurations. The variations of helical soil nails primarily consisted of different shaft types, shaft roughness, variation of number of helices (single, double, and triple), embedded nail length ratio, and embedment depth ratio. Furthermore, influence of installation torque is also examined thoroughly on parameters affecting pullout capacity of helical soil nails such as shaft diameter, shaft roughness, number of helices, overburden, helical pitch, and embedded helical nail length.

2 Pullout testing apparatus

The pullout testing apparatus was set up at Jaypee University of Information Technology, Waknaghat, Solan, Himachal Pradesh, India (Fig. 1). During pullout failure, helical soil nails are subjected to tension force which leads to mobilization of shear stresses along the pullout length embedded in the earth passive zone. For accurate modeling of this boundary value problem, a short helical nail length representative of actual nail segment within the passive zone can be used. The use of a shorter length also enables the use of uniform stress generation in place of non-uniform stresses, thereby simplifying the examination of installation torque and pullout capacity of helical soil nails [37]. Thus, a shorter nail length within a rectangular steel tank will simulate a uniform stress condition around the nail under passive earth pressure condition. In view of the above-stated reason, a steel tank of size 2 m long × 1.1 m wide × 1.1 m high is used. To avoid any boundary effect, least tank dimension (1.1 m) is taken as ten times greater than the maximum helix size (0.096 m) [10, 37]. Correspondingly, all other tank dimensions were determined such that there is no boundary effect on helical soil nail pullout behavior. In order to facilitate helical soil nail installation and pullout, a circular opening of 160 mm was made at the center of the front face of the tank. The tank walls were greased prior to filling with soil. The soil used in the present study is classified as poorly graded sand (SP). The other physical properties of the obtained soil are presented in Table 1. In accordance with the pluviation technique, sand was made to free fall from a height of 108 cm to achieve relative density (R_d) of 86.4% and a finished sample height of 1000 mm. The R_d of prepared sample is checked at various depths through sand replacement method.

A 65 ton (597.84 kN) capacity hydraulic jack against a steel reaction frame is used for applying vertical overburden pressure. The testing has been conducted under four different overburden pressures of 5 kPa, 12.5 kPa, 25 kPa, and 50 kPa applied on the top soil surface. For uniform

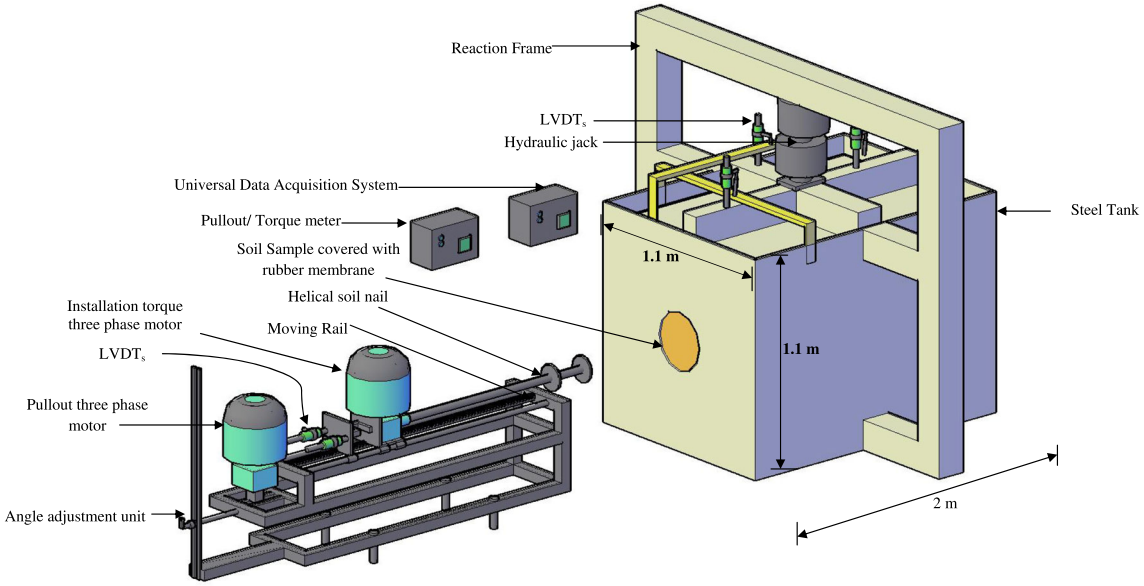

Fig. 1 Pullout system for soil nail

Table 1 Physical properties of sand

Property	Value
Specific gravity, G_s	2.72
D_{60} (mm)	0.28
Average grain size, D_{50} (mm)	0.25
D_{30} (mm)	0.21
Effective size D_{10} (mm)	0.16
Coefficient of uniformity, C_u	1.75
Coefficient of curvature, C_c	1
Friction angle from direct shear test, Φ (°)	37.9°
Maximum dry unit weight, $\gamma_{d(max)}$ (kN/m^3)	16.87
Minimum dry unit weight, $\gamma_{d(min)}$ (kN/m^3)	13.13
Relative density (R_D)	86.4%

D_{50} is the average grain size; D_{10}, D_{30}, and D_{60} are the soil grains diameter where 10%, 30%, and 60% of the particles are finer than this size, respectively

pressure distribution over soil surface, a steel plate of 10 mm thickness, welded with two I sections laterally and longitudinally to regulate any plate deformation during load application, is used. The filled soil tank along with the steel plate was left undisturbed for 24 h for development of in situ stresses at rest. The applied vertical pressure was measured by a load cell attached to the hydraulic jack. Four LVDTs to record vertical surface settlements during installation and pullout were also fixed in a square arrangement at distance of 15 cm around the hydraulic jack.

The installation of helical soil nails is carried out by the pullout/torque installation machine which comprises of two three-phase induction motor, each of 0.5 HP. One induction motor facilitates forward and backward helical nail movement, while the other provides the rotation during installation. The induction motor for installation consists of a drive head for providing the necessary torque and adapter of variable diameter for holding different nail shaft diameters. During installation, both motors are coupled together to render torque and crowd force for inserting the nail into the soil tank. The pullout of helical soil nail is done by locking the drive head and reversing the translational motion so as to create a pullout force measured using a 50 kN calibrated load cell. The maximum and minimum pullout displacement rate that can be achieved is 10 mm/min and 1 mm/min, respectively, as adopted from FHWA [8].

The setup is completely instrumented for recording real-time data of vertical displacement (i.e., top platen settlement) and horizontal displacement (i.e., pullout) using linear variable differential transformers (LVDTs). A total of six LVDTs were used in the present study with four on the top plate to measure vertical displacement, and two were located either side of nail head to measure horizontal displacement during helical nail pullout. The overburden pressure and pullout force are recorded using calibrated load cells. The stresses developed during installation and pullouts are also recorded using earth pressure cells embedded at specific locations during sample preparation. All the real-time data are recorded using a 30-channel (DLX-U-RS 232-USB series) Universal Data Acquisition System (UDAS).

3 Scaling and fabrication of helical soil nails

The scale effect on behavior of helical element specimens in granular soils is evaluated on the basis of two mechanisms: (1) effect of mean particle size on shaft resistance and (2) effect of mean particle size on helical bearing resistance [29]. For no scale effect on shaft resistance, the ratio of minimum shaft diameter (d) to mean grain size of soil (D_{50}) is given in Eq. (1) as:

$$\frac{d}{D_{50}} > 30 - 50 \tag{1}$$

However, for helical plate, d/D_{50} ratio is not considered as the appropriate factor for countering the grain size effects on helix resistance. The scale effects on resistance from helical plates along nail shaft are more often correlated to the effective radius of a helix (w_s) calculated using helix diameter (D_h) and shaft diameter (d) by Eq. (2) as:

$$w_s = \frac{D_h - d}{2} \tag{2}$$

Alternatively, for no scale effect on helical bearing resistance, Schiavon et al. [29] suggested that the ratio of effective radius of a helix (w_s) to mean grain size of soil (D_{50}) is given in Eq. (3) as:

$$\frac{w_s}{D_{50}} > 58 \tag{3}$$

Thus, for fabrication of helical soil nails in the present study with D_{50} of used soil as 0.25 mm, minimum shaft diameter comes out to be 12 mm such that $d/D_{50} = 48$ which lies within the range 30–50 (Eq. 1). Similarly, diameter of helices is adopted such that for a 12 mm nail shaft, the effective radius of helix [$w_s = 0.5(48–12)$] is 18 mm and the corresponding w_s/D_{50} ratio is 72, which is greater than 58 as per Eq. (2). Thus, abiding to both the norms, it is assumed that the installation and pullout results are not significantly under scale effect.

Under field conditions, the available helical nail shaft diameters are in the range of 38.1–88.9 mm with 152.4–355.6 mm helix diameter [9, 13]. Thus, using Eq. (4) as given by Rotte and Viswanadham [27] and adopting a scale factor (k) as 5, prototype nail shaft diameters are scaled down to obtain the nail shaft diameters for model helical soil nails

$$d_m = \frac{d_p}{k} \tag{4}$$

where d_m = diameter of the nail shaft used for model testing and d_p = nail shaft diameter in prototype. Hence, shaft diameters of 12 mm, 14 mm, 16 mm, and 18 mm for both solid and hollow shafts have been adopted in the present study. For hollow shafts, internal diameter is taken as external shaft diameter (d_0)—4 mm thickness (t). The variation of helix diameter ranges between 48 mm and 96 mm. The number of helical plates is varied from 1 to 3 with pitch variation in the range of 24.5–41 mm and thickness of 8 mm. The helical plates are welded along the nail length at regular spacing of three times the helix diameter (D_h). The adopted length of model helical soil nails (L) is calculated using the recommendation of $L = 0.7H$ [9] where H = wall height. For the present case, soil model has a height of 1000 mm which corresponds to a nail length of 700 mm to be used. The effective nail length, i.e., penetrated length of helical soil nail, in soil is taken as 700 mm with an additional length of 300 mm for fastening purposes. The nail head is beveled at an angle of 30° to facilitate penetration with first helical plate located at 20 mm from the nail head. All the helical soil nail and helix plate specimens were fabricated using mild steel. Three different types of circular shafts categorized as hollow shaft, solid shaft, and rough soil shaft were used for testing. Smooth surface was modeled using smooth mild steel solid and hollow bars. For rough surface deformed ribbed solid steel bars were used. The details of model helical soil nails are summarized in Table 2.

4 Testing program

The testing program encompasses 88 installation and pullout tests using different nail shaft types (i.e., hollow and solid shafts), variation in nail shaft and helical diameter, variation in number of helical plates, helical pitch, and embedment depth ratio (Z/D_h). The variation in helical soil nail configuration was used to examine the variation in installation torque, pullout capacity, earth pressure generation around the nail, and strains developed during installation and pullout. A comparative study between hollow and solid shaft helical soil nails has also been carried out to evaluate the most suitable shaft type. The testing program has been divided into five groups. The first group comprises of solid and hollow shafts of different shaft diameters varying from 12 to 18 mm. This group only consists of nails with one helix and constant pitch of 24.5 mm. Since the D_h/d ratio is taken as 4 for all model tests [9], helix diameter also varies from 48 to 72 mm. The first group has been used to find the most optimized nail based on shaft diameter. The second group consisted of only optimized helical nails obtained from the first group. The nails classified in the second group are tested for variation of helical pitch ranging from 30 to 41 mm. This enables optimization of helical pitch. Now with the optimized shaft diameter and helical pitch, optimization of number of helical plates is conducted under the third group of nails. The third group primarily involves optimized nails from the second group with double helices having equal diameter (64 mm) and

Table 2 Helical soil nails configurations

Sr. no.	Nail identification	Shaft type (mm)	Shaft diameter (mm)	Number of helices	Spacing/helix diameter (S/D_h)	$A_s = A_{helix} + A_{shaft}$ (mm^2)	Helix diameter, (D_h) (mm)	Pitch of helix (mm)	Embedment ratio (H/D)	Surface type	Overburden pressure (kPa)
	First group										
1	SS12-SH48P24.5	Solid	12	1	–	26489.04	48	24.5	10.4	Smooth	5, 12.5, 25, 50
2	SS14-SH56P24.5	Solid	14	1	–	30903.88	56	24.5	8.92	Smooth	5, 12.5, 25, 50
3	SS16-SH64P24.5	Solid	16	1	–	35318.72	64	24.5	7.8	Smooth	5, 12.5, 25*, 50
4	SS18-SH72P24.5	Solid	18	1	–	39733.56	72	24.5	6.9	Smooth	5, 12.5, 25, 50
5	HS12-SH48P24.5	Hollow	12	1	–	52865.04	48	24.5	10.4	Smooth	5, 12.5, 25, 50
6	HS14-SH56P24.5	Hollow	14	1	–	61675.88	56	24.5	8.92	Smooth	5, 12.5, 25, 50
7	HS16-SH64P24.5	Hollow	16	1	–	70486.72	64	24.5	7.8	Smooth	5, 12.5, 25, 50
8	HS18-SH72P24.5	Hollow	18	1	–	79297.56	72	24.5	6.9	Smooth	5*, 12.5, 25, 50
	Second group (SH64)										
9	SS16-SH64P30, P35.5, P41	Solid	16	1		35318.72	64	30, 35.5, 41	7.8	Smooth	5*, 12.5, 25, 50
10	HS16-SH64P30, P35.5, P41	Hollow	16	1		70486.72	64	30, 35.5, 41	7.8	Smooth	5, 12.5*, 25, 50
	Third group										
11	SS16-DH64e P30	Solid	16	2	3	35469.44	64 and 64	30	7.8	Smooth	5, 12.5, 25, 50
12	SS16-DH90e P30	Solid	16	2	3	35632.80	90 and 90	30	5.55	Smooth	5, 12.5, 25, 50
13	SS16-DH64n90P30	Solid	16	2	3	35551.12	64 and 90	30	5.55	Smooth	5, 12.5*, 25, 50*
14	SSRS16-DH64n90P30	Solid	16	2	3	35551.12	64 and 90	30	5.55	Rough	5, 12.5, 25*, 50
15	HS16-DH64n90P30	Hollow	16	2	3	70919.12	64 and 90	30	5.55	Smooth	5, 12.5, 25, 50
	Fourth group										
16	SS16-TH64n90n96P30	Solid	16	3	3	35802.44	64, 90 and 96	30	5.2	Smooth	5, 12.5, 25*, 50
17	HS16-TH64n90n96P30	Hollow	16	3	3	70970.44	64, 90 and 96	30	5.2	Smooth	5, 12.5, 25, 50
	Fifth group										
18	SS16	Solid	16	0	–	35168	–	–	–	Smooth	5, 12.5, 25, 50
19	HS16	Hollow	16	0	–	70336	–	–	–	Smooth	5, 12.5, 25, 50

SS solid shaft; *SS16* solid shaft of diameter 16 mm; *HS* hollow shaft; *HS16* hollow shaft of diameter 16 mm; *RS* rough surface; *SH* single helix; *SH48* single helix of dia. 8 mm; *DH* double helix; *DH64* double helix of diameter 64 mm; *TH* triple helix; e = each; n = and; P = pitch, TH64n90n96P30 = triple helix with 64 mm (diameter of front helix with 30 mm pitch) and 90 mm (diameter of middle helix with 30 mm pitch) and 96 mm (diameter of last helix with 30 mm pitch)

*Tests were repeated to check consistency of experiments

increasing diameter (64–90 mm) with constant pitch of 30 mm. The third group also consists of an additional nail configuration having rough surface solid shaft double helical nail (Fig. 2). The fourth groups deal with nails with triple helices of increasing diameter from 64 to 96 mm and constant pitch of 30 mm. The fifth group comprises of solid and hollow nail shafts of 16 mm without any helix for comparative evaluation. The details of different helical nail configurations adopted are given in Table 2.

4.1 Interface direct shear test

The basic mechanism of pullout resistance of helical soil nail is predominantly governed by the soil–nail interface friction. Previous studies [15, 36] have suggested that interface friction between soil and nail surface can be accurately predicted using a direct shear apparatus. In this study, small direct shear box (6 cm × 6 cm) was used to investigate both soil–soil and soil–nail interface friction values. For determination of interface friction of reinforced

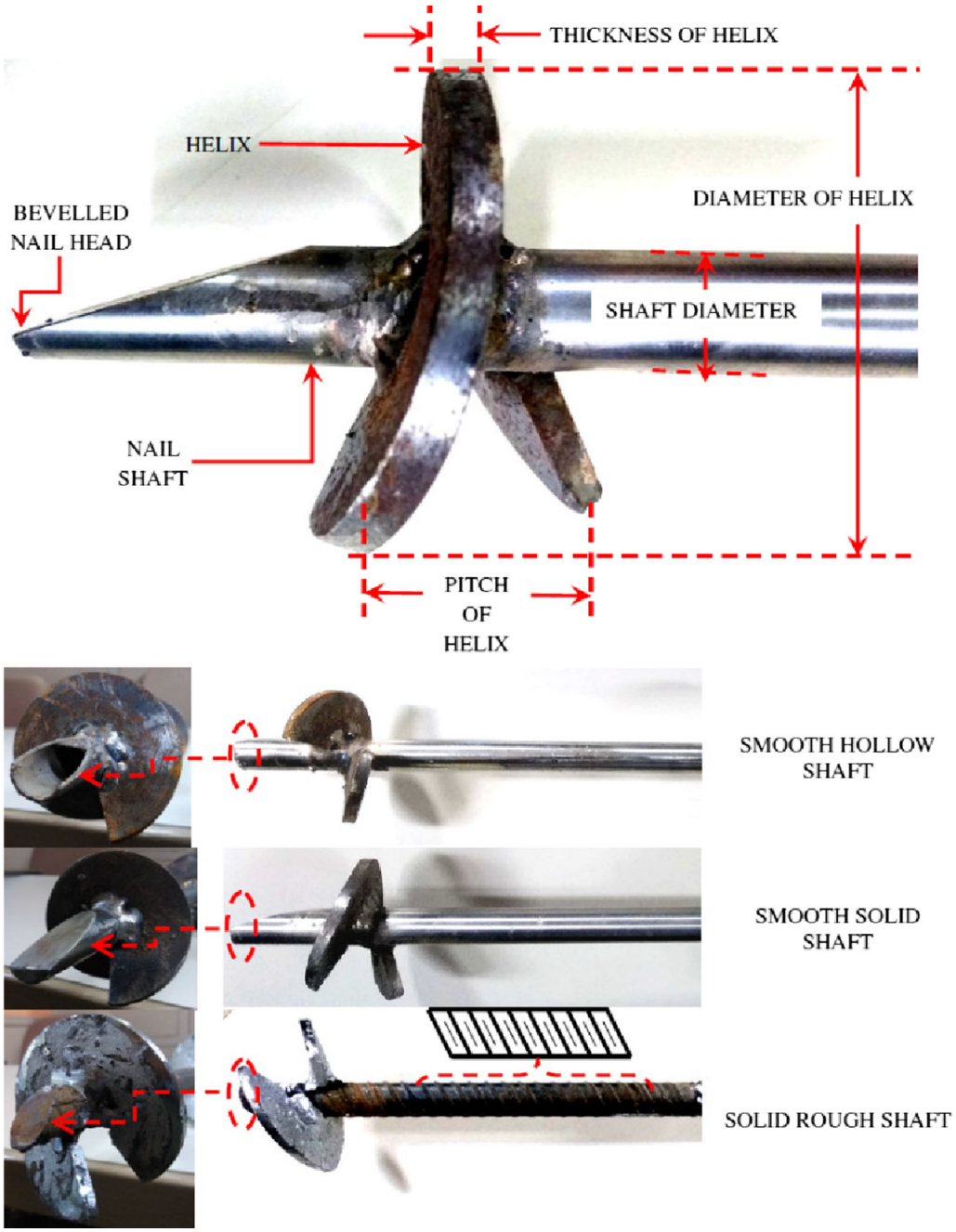

Fig. 2 Helical soil nails

soil, it is well documented [15] that the nail should be located in regions of incremental tensile strains developed in the soil during shearing. As suggested by Jewell and Wroth [15], this can be achieved by orienting the nail at an inclination of 25° ($\theta = 25°$) from the vertical (Fig. 3a). However, the direct shear test underestimates the mobilized interface friction value as compared to pullout testing [15, 36]. Moreover, results obtained from direct shear test are not axisymmetric because of the limitations associated with direct shear test apparatus. The stresses developed within the soil mass during shearing are non-uniform due to boundary effect from the apparatus. The principal plane before the test is treated as horizontal (i.e., with shear stress = 0). However, during shearing, the principal plane rotates which is difficult to quantify and hence rotation of principal plane at failure is determined by the internal

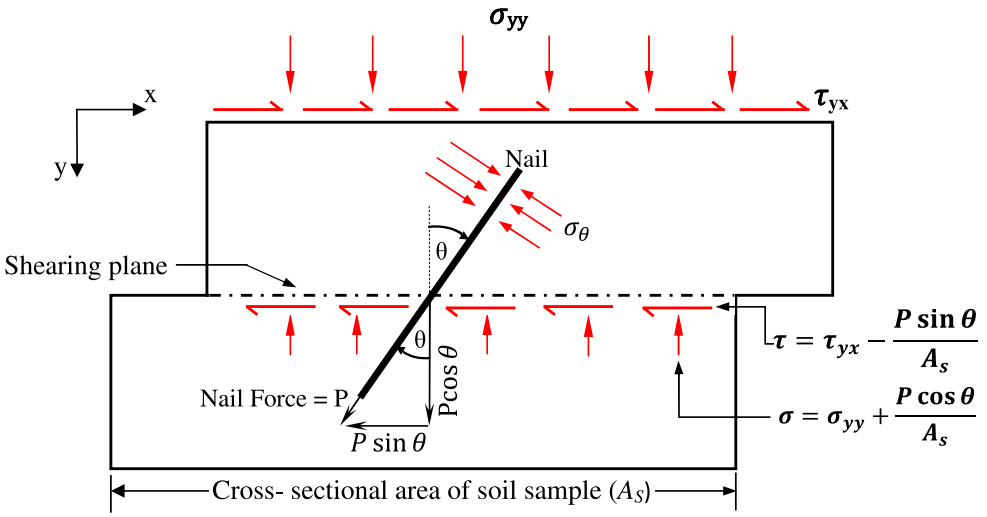

a Direct shear test for soil nail reinforced sand

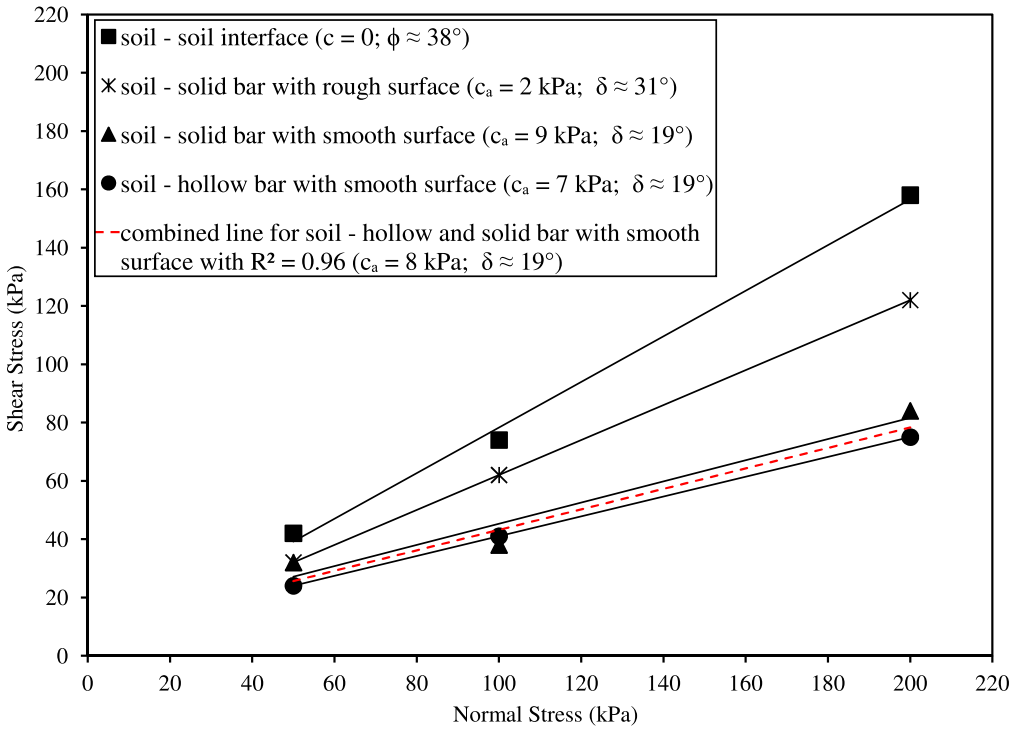

b Shear strength parameters.

Fig. 3 **a** Direct shear test for soil nail-reinforced sand, **b** shear strength parameters

angle of friction of soil [6, 15]. Similarly, when sand reinforced with nail is sheared, deformation of soil around the nail mobilizes additional shearing resistance due to nail. The soil in the vicinity of nail will try to undergo deformation with respect to nail. Since the ratio of stiffness of nail to soil is high and orientation of nail is in direction of incremental tensile strains in the soil, the soil deformations are resisted. This brings a transition in the state of stress of the adjoining soil. As a result, the principal plane of stresses rotates so that in situ equilibrium is attained for the generated shear stresses between deforming soil and resisting nail element [15]. Thus, for simplifying the stress conditions during direct shear test, plain strain conditions are normally assumed [15] as in the present scenario. The plane strain condition can significantly help solve problems associated with earth pressure and slope stability problems. However, axisymmetric testing conditions using triaxial testing are recommended for application of results for bearing capacity problems.

4.2 Installation of helical nails and pullout testing

The novelty of the present work primarily lies in the fact that this study investigates the installation effects on pullout behavior of different configurations of helical soil nails. The helical soil nails were installed at desired depth using a drive head rotating at a rate of 10 rpm with a crowd force supporting a rate of penetration of one helix pitch in one revolution [9, 13]. All helical nails were installed up to an effective embedded length of 700 mm in the soil with nail inclination of 0° to the horizontal. The installation was carried under varying overburden pressures of 5 kPa, 12.5 kPa, 25 kPa, and 50 kPa. The main reason for using overburden pressure ranges below the normal stresses as used for direct shear testing is due to the fact that a normal stress of 150 kPa models a fill of height 6–7 m which has been adopted by previous researchers for pullout study of conventional soil nails [16, 21]. However, in the present study, during installation and pullout overheating of hydraulic jack during sustained load application for long periods imposed a restriction of applying a maximum overburden pressure of 55 kPa only. The low overburden pressure facilitates development of low stress as found during phased or staged construction procedure. Moreover, since a Mohr–Coulomb failure criterion was adopted for assessment of interface behavior of reinforced soil, interface shear (τ) and normal stress (σ_n) conditions for lower normal stresses of 5 kPa, 12.5 kPa, 25 kPa can easily be extrapolated by the τ/σ_n line. Moreover, it is observed that during pullout testing, the overburden pressure applied is increased due to the additional confining stress generated by the restrained volume expansion of the soil. This additional confining results in mobilization of greater frictional angle as deduced from direct shear test. Also, higher bond stresses mobilized in pullout tests are much identical for field loading conditions [15]. The installation torque is recorded by a torque meter in real time for the entire embedded length of helical soil nail. The installed nail was left for 24 h to attain equilibrium in situ stress conditions. After a seating period of 24 h, displacement-controlled pullout testing of installed helical soil nail was carried out by applying the crowd force in the reverse direction so as to create a pull on the helical soil nail. The maximum and minimum pullout displacement rates of 10 mm/min and 1 mm/min, respectively, that can be achieved are adopted as per FHWA [8]. For the present pullout testing, pullout force was applied at a rate of 1 mm/min on each nail until a total horizontal displacement of 90 mm was reached. The termination of pullout test on reaching a horizontal displacement of 90 mm was based on the norm that in displacement-controlled pullout test, ultimate pullout force can be taken as either the maximum peak value or the point where increment in force per 1 mm displacement is less than 1% or a point where displacement reaches to 30 mm [8, 38]. Similar to the installation torque measurement, real-time pullout force with horizontal nail displacement was continuously measured during the testing.

5 Results and discussion

5.1 Direct shear test

It can be seen from Fig. 3b that soil–soil interface depicts a higher Mohr–Coulomb failure envelops in comparison with reinforced soil interfaces of soil–solid rough shaft; soil–solid smooth shaft; and soil–hollow smooth shaft. This indicates that during failure, shear strength parameters of soil–nail interface will be mobilized prior to soil–soil interface. This phenomenon can be understood from Fig. 3a which depicts the effect of reinforcement element, i.e., additional increase in normal stress which consequently increases the overall shearing resistance [15] which is given in Eq. (5) as:

$$\tau_{\text{reinforcement}} = \frac{P}{A_S}(\cos\theta\tan\phi + \sin\theta) \tag{5}$$

The additional shearing resistance is mobilized only when mobilized angle of internal friction (ϕ) denoted by 'tan ϕ' component in Eq. (5) is reached. Thus, from Fig. 3b, it can be seen that under same state of stress as for unreinforced (soil–soil) condition, soil–solid nail with rough surface is mobilized at $\delta_i = 31°$ much before than the mobilization for soil–soil interface having $\phi = 38°$. Thus,

additional shearing resistance due to nail element mobilizes both the adhesion and interface friction components, thereby increasing the overall shear strength of the composite soil. For both soil–solid bar and soil–hollow bar with smooth surfaces, it is observed that additional shearing due to nail as denoted by Eq. (5) is mobilized at $\delta_i = 19°$. However, the increase in shear strength is found to be more for solid bars as compared to hollow bars due to the increased adhesion obtained for solid bar nail. Moreover, it can be inferred that adhesion decreases and interface friction increases with the increase in surface roughness. It can also be deduced that with introduction of reinforcing element (nail) in soil under shearing state, the decrease in interface friction angle enables early mobilization of nail forces which generates additional shearing resistance, thus increasing the shear strength of reinforced soil. In the absence of the reinforcing element, under the same shearing state, mobilization of peak angle of internal friction will occur rapidly under low tensile strains resulting in soil failure. Thus, the mobilization of stresses on the soil–nail interface is investigated in terms of a non-dimensional factor called the interface reduction factor (f_δ). The interface reduction factor is defined as ratio of soil–nail interface friction angle ($\delta_i°$) to angle of internal resistance of soil ($\phi°$). Wang and Richwien [36] suggested $f_\delta < 0.5$ for a smooth surface and $f_\delta > 0.8$ for a rough surface. In present study, f_δ for different interfaces used is summed up in Table 3. It can be seen that f_δ values for rough and smooth shaft (solid and hollow) are within the recommended limits [36]. Consequently, it can also be inferred that with use of smooth hollow and solid nail shafts in soil, shearing will be taken up by the reinforcement as soon as 50% of angle of frictional resistance of soil is mobilized. This clearly reflects that with the increase in shaft roughness, an increased soil–nail interaction is attained.

5.2 Effect on installation torque

The various parameters influencing the installation torque include friction angle of soil, interface friction between soil and nail, unit weight of soil, relative density, and particle size of soil. With reference to helical nails, shaft type, shape and roughness, shaft diameter, helix diameter and thickness, number of helices, pitch of helices, and installation method also influence the torque applied. Consequently, installation torque affecting the uplift or compressive capacities of helical piles and anchors has also been reported by many researchers [12, 14, 19, 22, 28]. Hoyt and Clemence [12] also developed a correlation between pullout capacity and installation torque for vertically installed helical anchors and piles as given in Eq. (6)

$$Q_u = K_t T \tag{6}$$

where K_t = empirical factor; Q_u = pullout capacity (kN) and T = average installation torque (kN-m). As per design manuals developed for helical systems [9, 13, 14], it is reported that Eq. (6) can also be used for horizontal helical systems. However, the authors were unable to list any published literature for case of helical soil nails. Hence, from the testing results obtained, a relation between installation torque and pullout capacity for horizontally installed helical nail under different surcharge pressures has been developed. During installation of a helical soil nail, frictional resistance and penetration resistance act on the helical plate and nail shaft against the lateral stress ($K\sigma_v$). As shown in Fig. 4 (Section C–C'), it can be seen that frictional resistance acts on the helix and increases with square of helix diameter [14]. Additionally, frictional resistance also acts along the helical perimeter and is governed by the thickness of helical plate. Moreover, frictional resistance also increases with the increase in helical pitch. A helix with large pitch will have to slice against large volume of soil, and thus, work required against soil friction resistance will also be more. The other component of frictional resistance acts along the helical shaft during installation. The frictional resistance depends on the surface area of shaft in contact with the soil during installation. With the most efficient torque transmission capacity and having complete surface area in contact with the soil, a circular nail shaft therefore requires significant installation energy. Thus, the total frictional energy or energy loss required during helical soil nail installation depends on the helix and nail shaft size as given in Eq. (7):

$$\begin{aligned}&\text{Energy Loss}_{(\text{Friction})}\\ &= \sum \text{Energy loss of Individual helix}_{(\text{Friction})}\\ &\quad + L_{(\text{shaft in friction})}\end{aligned} \tag{7}$$

Simultaneously, penetration resistances are found to act on the leading edge of helix and beveled nail head. The size of the leading edge is determined by the adopted helix diameter and thickness. As the leading edge cuts through the soil, passive shearing resistance is mobilized. It is observed that as the helix cuts through the soil, it displaces a soil volume equal to half of the helix thickness [14]. This

Table 3 Interaction of different soil–nail interfaces from direct shear test

Type of interface	Interface reduction factor $f_\delta = \frac{\delta_i}{\phi}$
Soil–rough surface solid bar	0.82
Soil–solid bar with smooth surface	0.50
Soil–hollow bar with smooth surface	0.49

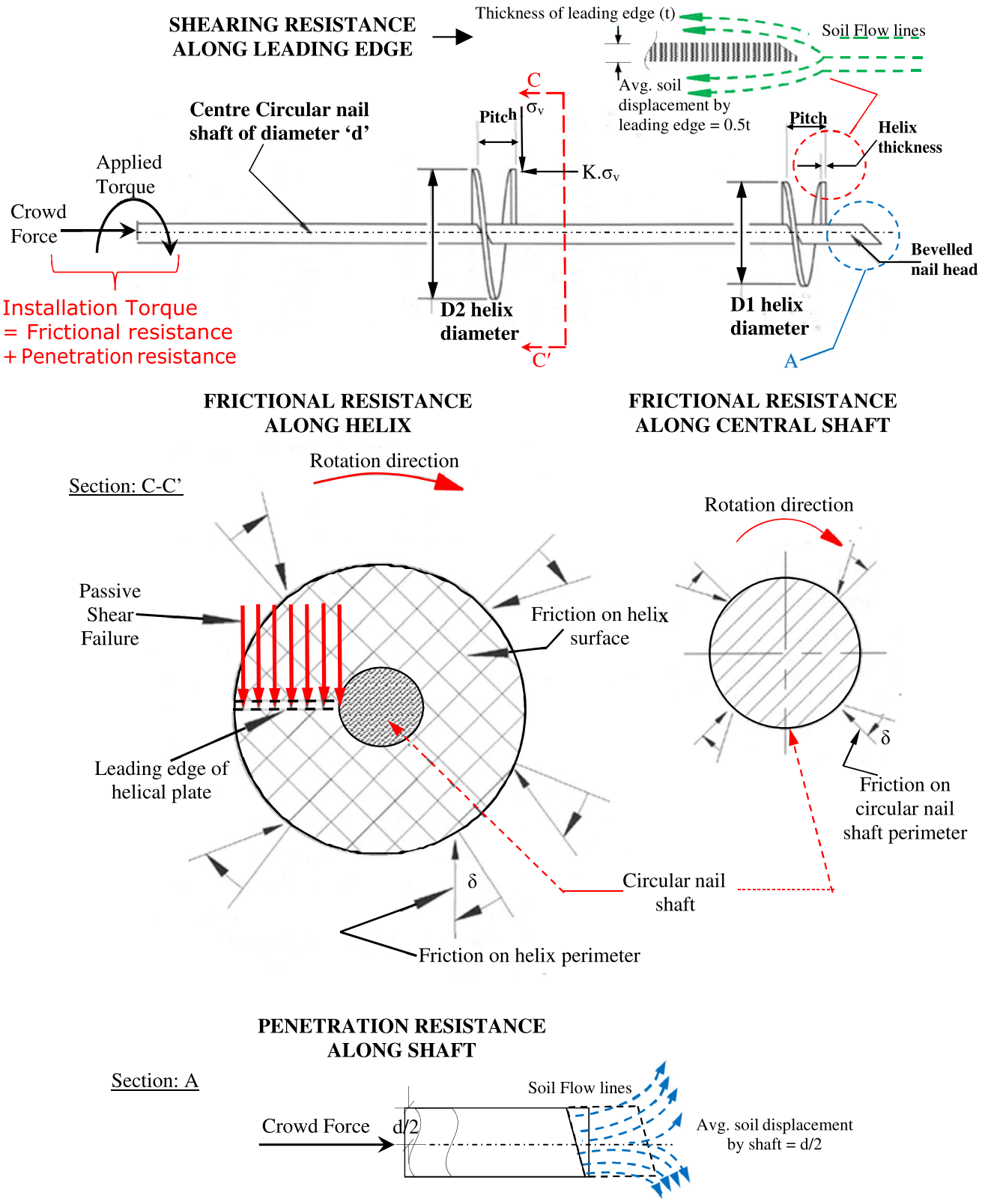

Fig. 4 Various forces acting on helical soil nail during installation

clearly denotes that for obtaining minimum disturbances during installation, thickness of helix should be less. The second component of penetration resistance acts on the c/s area of beveled nail head. As the shaft diameter increases,

the projected area of the nail head will also increase, and consequently, penetration resistance increases with the square of shaft diameter. It is observed that nail head displaces soil volume corresponding to half of the shaft diameter [Fig. 4 (Section: A)]. Thus, large shaft diameter will require greater displacement of soil volume and correspondingly greater work to be done. The total penetration energy per rotation thus required is given in Eq. (8) as:

$$\begin{aligned}&\text{Energy}_{(\text{Penetration})}\\&=\sum \text{Soil volume displaced by each helix}\\&\quad+\text{Soil volume displaced by nail head}\end{aligned} \tag{8}$$

Hence, installation energy is required to overcome the frictional and penetration resistances. The drive head installed in the installation/pullout unit provides the required rotational energy and crowd force (forward push). The rotational energy generates the required thrust to overcome the resistances (frictional and penetration resistances) and is called as 'installation torque.' The crowd force is generally required only during the start of installation and during penetration of nail from soft to hard soil strata.

For vertically installed helical anchors and piles, the installation torque used for prediction of uplift capacity is generally averaged over a depth of three times the average helix diameter or the last torque value is adopted [12, 22]. The reason for adopting this installation torque is attributed to the fact that as helical anchor penetrates to a greater depth or moves from soft to hard soil stratum, the vertical stress (σ_v) increases with depth and consequently increases the lateral pressure on the helical plates. Thus, during installation of final helical plate to the desired depth, significant increase in torque is required. To compensate for the variation in torque values due to changing soil stratum and other installation asperities such as auguring and untrue helix shape, the installation torque is averaged. However, as per FSI [9], adopting the final or last installation torque reading is debatable and therefore torque during entire installation should be recorded. In the present study, the installation torque for entire helical soil nail length of 700 mm has been recorded continuously and is used for obtaining the maximum installation torque (T_{max}). Since a homogeneous soil without any stratification and constant relative density has been used for the entire model testing program, the maximum installation torque obtained during nail installation has been considered as critical. Another reason for adopting T_{max} value as critical is attributed to the constant lateral earth pressure ($K\sigma_v$) experienced by the helical plates and nail shaft during penetration due to constant vertical stress (σ_v) for a horizontal nail unlike vertical anchors. Thus, for determining K_t, Eq. (6) has been modified by using maximum installation torque (T_{max}) values for different nail configurations and correlating it to the maximum pullout capacity [$Q_{u(max)}$] as given in Eq. (9):

$$Q_{u(max)} = K_t T_{max} \tag{9}$$

where K_t = empirical factor (m^{-1}); $Q_{u(max)}$ = maximum pullout capacity of helical soil nail (kN); and T_{max} = maximum torque during installation (kN-m). Using Eq. (9), K_t for helical soil nails with solid shaft is found in the range of 19–61 m^{-1}. Similarly, for helical nails with hollow shafts, K_t is found in the range of 23–58 m^{-1}. The K_t values for different nail configurations under varying overburden pressures are summarized in Table 4. For combined case of solid and hollow shaft, K_t is evaluated based on the fact that $Q_{u(max)}$ and T_{max} are related by a linear relationship, where the slope of the line will represent the K_t value (Fig. 5). Based on this, a best fit line (R^2 = 0.89) is predicted for combined hollow and solid shaft nails under overburden pressure of 50 kPa rendering a K_t = 28.77 $m^{-1} \approx 28.8$ m^{-1} and given in Eq. (10):

$$Q_{u(max)} = 28.8 T_{max} + 0.7 \tag{10}$$

It can be also noted from Tables 2 and 4 that as embedded nail area increases, K_t decreases for both solid and hollow shaft nails with single helix. The embedded helical nail surface area (A_s) in mm^2 is calculated using Eq. (11) given as:

$$A_s = A_{helix} + A_{shaft} \tag{11}$$

where A_{helix} = surface area of helix (mm^2) and A_{shaft} = surface area of the nail shaft (mm^2) which are determined using Eqs. (12) and (13) as suggested by [35] as:

$$A_{helix} = \pi\left[\frac{D_h^2 - d^2}{4}\right] \tag{12}$$

$$A_{shaft} = \pi d \times L_s \tag{13}$$

where D_h = diameter of helix; d = shaft diameter; and L_s = effective helical nail length of 700 mm.

The decrease in K_t value can be attributed to the increased installation torque required. For better understanding of this concept, variation of K_t is evaluated with the increase in nail shaft diameter. Hoyt and Clemence [12] reported that for helical anchors, K_t is a constant but depends mainly on shaft diameter. Based on the similar inference, Perko [22] developed a new empirical model wherein K_t was predicted to be a function of effective shaft diameter evaluated through a power law regression analysis. The reported literature clearly suggests that shaft friction dominates the contribution to both pullout and installation torque with only minor contribution from helix size. As the shaft diameter increases, correspondingly helix diameter increases, which reduces the shaft friction

Table 4 Maximum installation torque and pullout capacity values for different nail configurations under different overburden pressures

Nail identification	5 kPa				12.5 kPa				25 kPa				50 kPa				Shear stress	
Solid shaft helical nail	T_{max} (kN-m)	$Q_{u(max)}$ (kN)	$K_t = \frac{Q_{U(max)}}{T_{max}}$ $[m^{-1}]$	IF	T_{max} (kN-m)	$Q_{u(max)}$ (kN)	$K_t = \frac{Q_{U(max)}}{T_{max}}$ $[m^{-1}]$	IF	T_{max} (kN-m)	$Q_{u(max)}$ (kN)	$K_t = \frac{Q_{U(max)}}{T_{max}}$ $[m^{-1}]$	IF	T_{max} (kN-m)	$Q_{u(max)}$ (kN)	$K_t = \frac{Q_{U(max)}}{T_{max}}$ $[m^{-1}]$	IF	tanδ	c_a
SS12-SH48P24.5	0.05	1.92	36.23	14.50	0.06	2.51	41.15	7.58	0.08	2.93	38.15	4.42	0.09	3.58	39.69	2.70	0.75	52.13
SS14-SH56P24.5	0.07	2.32	33.62	15.01	0.08	3.04	36.63	7.87	0.12	3.63	31.57	4.70	0.13	4.44	34.15	2.87	0.81	55.32
SS16-SH64P24.5	0.09	2.86	31.78	16.20	0.11	3.80	34.55	8.61	0.15	4.65	31.00	5.27	0.18	5.60	31.64	3.17	0.86	62.05
SS18-SH72P24.5	0.11	3.30	30.00	16.61	0.14	4.15	29.64	8.36	0.17	5.05	29.71	5.08	0.21	6.28	29.90	3.16	0.92	60
SS16-SH64P30	0.07	3.10	43.66	17.55	0.12	4.13	34.42	9.35	0.15	5.00	33.33	5.66	0.18	6.00	32.61	3.40	0.89	71.22
SS16-SH64P35.5	0.07	3.15	43.15	17.84	0.13	4.19	33.52	9.49	0.16	5.09	31.04	5.76	0.18	6.10	33.80	3.45	0.85	68.50
SS16-SH64P41	0.08	3.00	38.41	16.99	0.13	3.95	31.32	8.95	0.17	4.70	27.17	5.32	0.19	5.95	31.32	3.37	0.83	69.42
SS16-DH64eP30	0.15	3.42	22.50	19.28	0.22	4.09	18.61	9.23	0.23	5.80	25.22	6.54	0.24	8.45	35.50	4.76	0.82	81.55
SS16-DH90eP30	0.18	3.63	20.74	20.37	0.25	4.75	19.07	10.66	0.27	6.23	23.07	6.99	0.26	9.23	35.23	5.18	0.89	82.12
SS16-DH64n90P30	0.15	5.07	33.80	28.52	0.17	7.02	41.29	15.80	0.19	9.68	50.95	10.89	0.22	12.70	57.73	7.14	0.98	106.17
SSRS16-DH64n90P30	0.16	6.00	37.50	33.75	0.18	8.30	46.11	18.68	0.20	10.63	53.15	11.96	0.23	13.23	58.28	7.44	0.99	109.8
SS16-TH64n90n96P30	0.17	6.80	40.00	37.99	0.19	9.20	48.42	20.56	0.21	11.50	54.76	12.85	0.23	14.00	60.87	7.82	0.99	93.45
SS16	–	1.20		5.69	–	1.63		3.71	–	1.67		1.90	–	2.10		1.14	0.39	14.52
Hollow shaft helical nail	T_{max} (kN-m)	$Q_{u(max)}$ (kN)	$K_t = \frac{Q_{U(max)}}{T_{max}}$ $[m^{-1}]$	IF	T_{max} (kN-m)	$Q_{u(max)}$ (kN)	$K_t = \frac{Q_{U(max)}}{T_{max}}$ $[m^{-1}]$	IF	T_{max} (kN-m)	$Q_{u(max)}$ (kN)	$K_t = \frac{Q_{U(max)}}{T_{max}}$ $[m^{-1}]$	IF	T_{max} (kN-m)	$Q_{u(max)}$ (kN)	$K_t = \frac{Q_{U(max)}}{T_{max}}$ $[m^{-1}]$	IF	tanδ	c_a
HS12-SH48P24.5	0.05	1.42	28.40	5.37	0.05	1.87	37.40	2.83	0.07	2.34	33.43	1.77	0.08	2.90	37.18	1.10	0.47	17.68
HS14-SH56P24.5	0.06	1.74	31.64	5.64	0.07	2.42	34.57	3.14	0.10	3.00	30.00	1.95	0.13	3.88	29.85	1.26	0.60	22.05
HS16-SH64P24.5	0.07	2.00	30.63	5.67	0.09	2.68	29.39	3.04	0.13	3.43	27.01	1.95	0.17	4.28	25.48	1.21	0.72	15.64
HS18-SH72P24.5	0.09	2.54	28.22	6.41	0.11	3.32	29.38	3.35	0.15	4.23	28.20	2.13	0.18	5.10	28.49	1.29	0.74	17.89
HS16-SH64P30	0.06	2.19	34.22	6.21	0.09	2.87	31.89	3.26	0.13	3.75	29.76	2.13	0.17	4.51	27.33	1.28	0.81	16.28
HS16-SH64P35.5	0.07	1.98	30.46	5.62	0.09	2.76	30.33	3.13	0.13	3.63	28.36	2.06	0.17	4.55	27.58	1.23	0.75	17.98
HS16-SH64P41	0.07	1.77	25.65	5.02	0.10	2.51	26.06	2.85	0.13	3.33	24.74	1.89	0.18	4.26	23.48	1.18	0.67	14.74
HS16-DH64n90P30	0.10	3.00	30.00	8.48	0.12	4.50	38.79	5.09	0.14	6.40	45.71	3.62	0.17	8.85	52.06	2.50	0.65	25.15
HS16-TH64n90n96P30	0.08	4.00	51.28	11.27	0.10	5.00	49.50	5.64	0.13	7.00	54.26	3.95	0.16	9.50	58.28	2.68	0.60	25.30
HS16	–	0.87		2.47	–	0.96		1.09	–	1.00		0.57	–	1.28		0.35	0.14	7.55

All helical soil nails are installed at rate of 10 rpm with rate of penetration equal to one helix pitch in one revolution

contribution. Perko [22] mentions that at extreme shaft diameter values, significantly large capacity-to-torque ratio is obtained both from theoretical and empirical relationships due to the reason that friction along the shaft becomes negligible. Hence, during installation of helical soil nails, as the shaft diameter increases from 12 to 18 mm, the component of shaft friction reduces, whereas friction and resistance due to large helix size increase. Thus, large penetration energy and surface area disturb the soil enough, resulting in friction along the shaft to become negligible and evidently the reduced K_t (Fig. 6). However, it does not reflect that large shaft diameters are not capable of producing high load capacity, but it only means the installation energy must be significantly large for installation of that helical nail.

However, during pullout, shearing mainly occurs at the edge of the helical plates. The translational motion during pullout is governed by frictional resistance acting at the surface area of the newly formed cylindrical shape of nail of enlarged diameter (i.e., equal to diameter of helix). This increases the pullout capacity of helical soil nail with larger shaft diameter, but the increase is less as compared to the increase in required installation torque. The difference in increase in installation torque to pullout capacity can be attributed to factors such as crowd force increases with square of pitch to shaft radius ratio [14] and large torque required for maintain constant rate of rotation for large shaft diameter [3]. As shown in Fig. 6, relationship between K_t and shaft diameter is weakly correlated rendering $R^2 = 0.514$ only. However, decrease in K_t with the increase in shaft diameter has also been reported in previous studies on helical anchors by Hoyt and Clemence [12] and Perko [14]. Based on the observations, a power regression relationship can be established between K_t and helical soil nail shaft diameter (d) as given in Eq. (14):

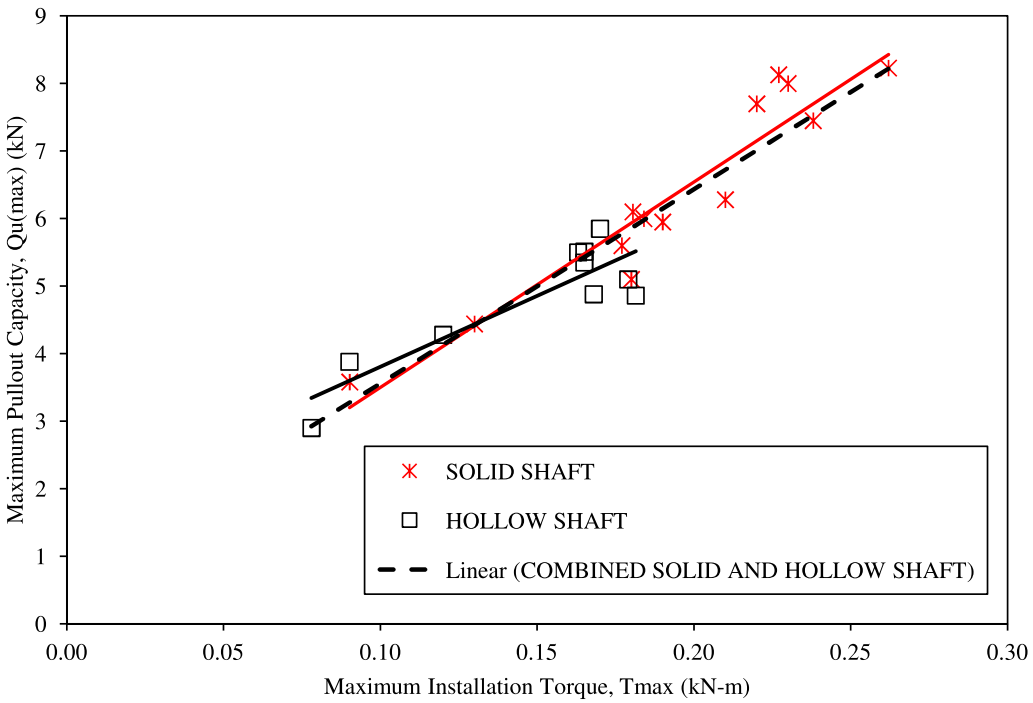

Nail type	Regression equations	R^2 value
Solid shaft nail	$Q_{u(max)} = 30.4T_{max} + 0.5$	$R^2 = 0.90$
Hollow shaft nail	$Q_{u(max)} = 21T_{max} + 1.7$	$R^2 = 0.78$
Combined solid and hollow shaft	$Q_{u(max)} = 28.8T_{max} + 0.7$	$R^2 = 0.89$

Fig. 5 Relationship between maximum pullout capacities and maximum installation torque

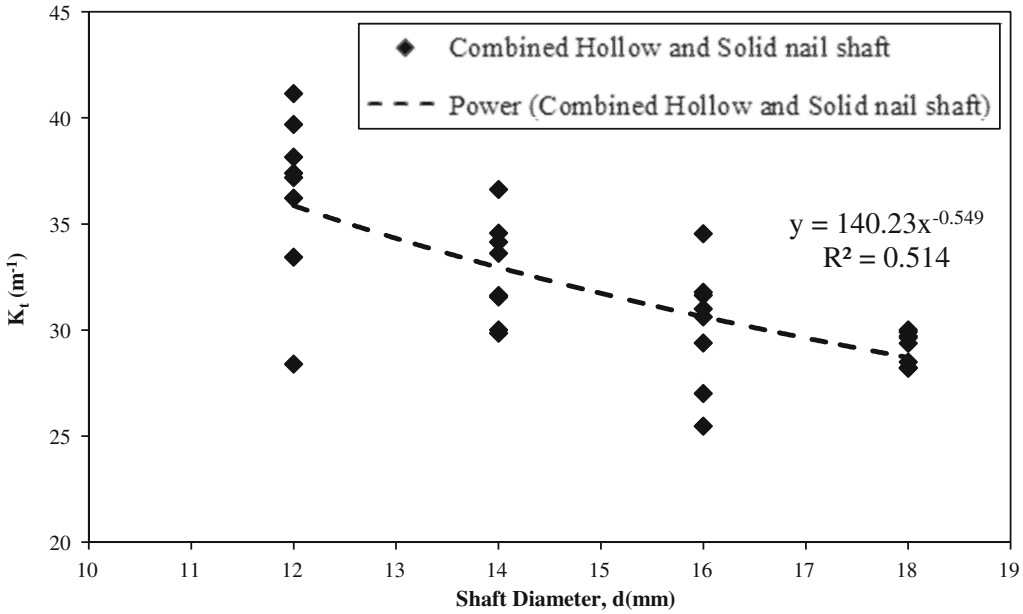

Fig. 6 Variation of K_t with shaft diameter

$$K_t = \frac{140.2}{d^{0.54}} \quad (14)$$

However, the low correlation between K_t and shaft diameter can be attributed to the limited range of shaft diameter (12–18 mm) used in the study.

Simultaneously, test results (Table 4) also reflect that overburden pressure, shaft type (solid and hollow), helix pitch, shaft roughness, and number of helices have a major effect on the installation torque. To examine the variation of installation torque with overburden pressure and change in helical soil nail geometry, non-dimensional parameters have been used for quantifying the wide variations in obtained values. The normalized installation torque [$T_{(max)}/T_0$] has been used for quantifying the maximum installation torque values of different solid and hollow shaft helical nail configurations. Normalized installation torque is defined as the ratio of maximum installation torque of different nail configurations to the maximum installation torque of SS12-SH48P24.5 for solid shaft and HS12-SH48P24.5 for hollow shaft helical soil nails. As shown in Fig. 7, with the increase in shaft diameter, $T_{(max)}/T_0$ also increases. A similar variation is observed with the increase in number of helices from single to double. However, $T_{(max)}/T_0$ for solid shafts is greater than hollow shafts and is found to increase with overburden pressure from 5 to 12.5 kPa and falls off gradually as overburden reaches 50 kPa.

Alternatively, another non-dimensional parameter (D_h/d) defined as the ratio of helix diameter to shaft diameter is used for investigating the torque efficiency of a helical element as an increasing D_h/d ratio reflects a better torque efficiency [14]. It is observed that the maximum installation torque is also found to increase with the increase in D_h/d ratio for solid shafts than hollow shafts and with increasing number of helices. Thus, it can be inferred that solid shaft helical nail with triple helices is the most efficient (best performing nail) in context of torque transmission as compared to hollow shaft helical soil nails with single, double, or triple helices. During installation of helical soil nail, soil displacement by the leading edge during rotation and by the nail head during forward advancement also governs the required installation torque. The size of the leading edge is dependent on the helix size which in turn is a function of shaft diameter. The distance between leading edge and trailing edge of helix is defined by its pitch. This means that with greater pitch, the leading edge has to travel a larger distance as it transverses the soil and is thus subjected to a greater shearing resistance. In order to evaluate the effect of penetration resistance during helical nail installation, maximum installation torque has been evaluated against a non-dimensional parameter defined as the ratio of helix diameter to helix pitch (D_h/P). The maximum installation torque with single helix is found be maximum for a D_h/P ratio of 1.6. The maximum installation torque decreases as D_h/P ratio increases from 1.6 to 2.1. However, beyond D_h/P ratio of 2.1, the maximum torque decreases. This variation can be explained on the basis that less installation energy is required for less work done (shorter path in slicing of soil) against resistance by helix of small pitch with same helix diameter. Now as the helix diameter increases with same pitch, friction from helix surface and corresponding more soil volume

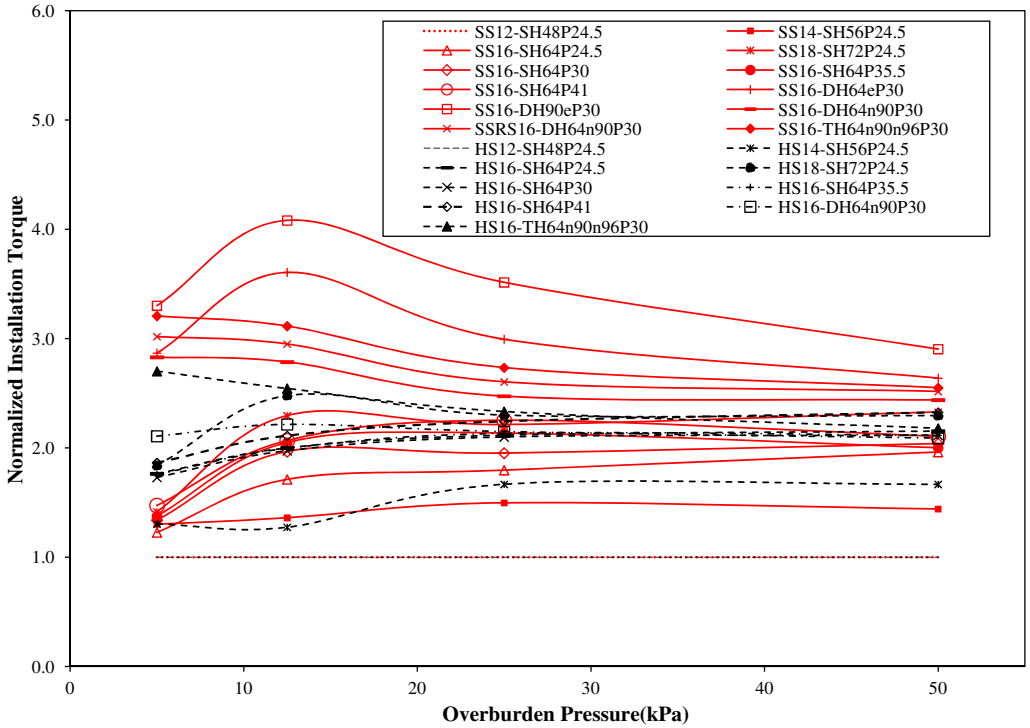

Fig. 7 Variation of normalized installation torque with overburden pressure

displacement from large nail shaft increases the required installation torque.

Similarly, the helical soil nail installation behavior is significantly influenced by the nail depth. The soil disturbances caused by helical nail installation can be attributed to the advancement of nail shaft and rotation of helical plates. As the helical plate transverses through the soil, it creates spiral-shaped cuts at regular pitch distances. Thus, the soil is displaced and sheared both laterally and vertically [2]. As the leading helical plate transverses the soil by radial soil displacement at the edge of helical plate, it reduces the in situ soil strength and stiffness. In case of similar helix diameter, no further soil strength and stiffness reduction will occur as the following helix traces the existing path. However, as the diameter of following helix increases, it cause more disturbances as compared to the helix, thereby further reducing in situ soil properties. Thus, most critical disturbances are caused by the largest helix diameter. With this view, varying H/D_h defined as ratio of horizontal depth of helical soil nail from installation end to the largest helix diameter (90 mm) is therefore used to depict the incremental shearing strain during installation [18]. As shown in Fig. 8a, the irregular (zig-zag) variation can be accounted for the strain-softening phenomenon occurring in the soil during nail installation for both cases of hollow and solid shafts. Generally, strain-softening phenomenon is characterized by a loss in resistance with continuous shearing after a peak resistance has been reached and is depicted by stress–strain behavior of soil.

Similarly, during helical nail installation, the torsional shearing stress is mobilized due to rotatory motion of the helical soil nail. As the helical nail installation progresses, the turning force attains a position where the rate of change of peak value shifts from positive to negative with continuous shearing. The phenomenon is also recorded during observation of installation torque which can be related to torsional shearing stress (τ_T) by principle of basic mechanics as given in Eq. (15):

$$\tau_T = \frac{16T}{\pi D_h^3} \tag{15}$$

where T = installation torque (kN-m) and D_h = diameter of the largest helix. Moreover, the incremental shearing strain during installation can also be studied in terms of normalized embedded length (ΔL/L) which also represents rate of change of length during installation. However, this ratio only reflects the strains mobilized due to advancement of nail shaft. Therefore, Fig. 8b depicts the stress–strain behavior of soil during helical soil nail installation in terms of torsional stress with normalized embedded length. It can be seen from Fig. 8b that strain-softening phenomenon occurs with increasing normalized embedded length. The variation is analogous to the plot of installation torque and H/D_h ratio.

5.3 Pullout behavior

5.3.1 Solid and hollow shaft with a single helix

It is observed from Fig. 9 that maximum pullout capacity increases with the increase in overburden pressure from 5 to 50 kPa for all types of solid and hollow shaft helical nails. This can be accounted for the fact that as overburden increases, large shear stress is generated around the nail shaft. As the pullout progresses, these induced shear stresses along with tensile stresses generated within the bar act against the pullout force. Figure 9 also indicates that pullout strength of solid shaft helical soil nail is greater than the hollow shaft helical soil nail. As evident from Table 4, the average pullout capacity for SS12-SH48P24.5 to SS14-SH56P24.5 and SS14-SH56P24.5 to SS16-

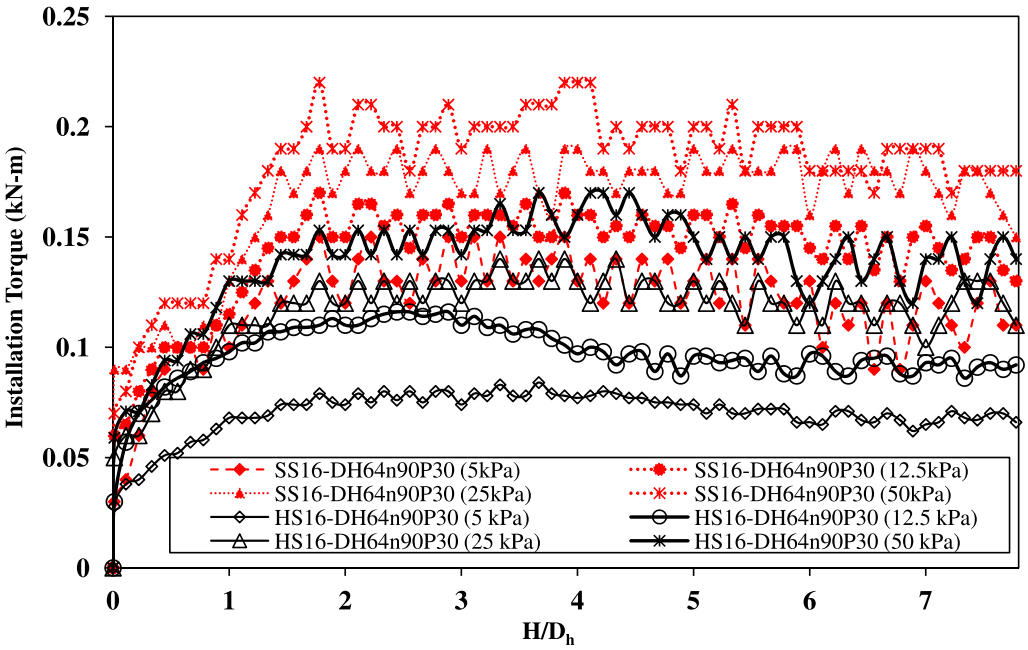

a Variation of Installation torque with H/D_h ratio

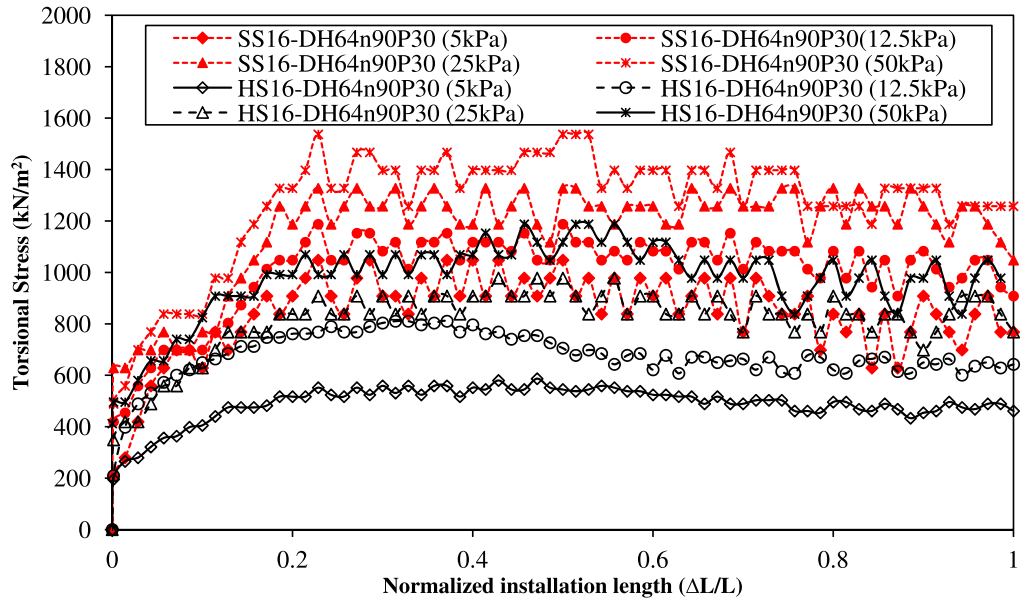

b Variation of Torsional Stress with Normalized installation length

Fig. 8 **a** Variation of installation torque with H/D_h ratio, **b** variation of torsional stress with normalized embedment length

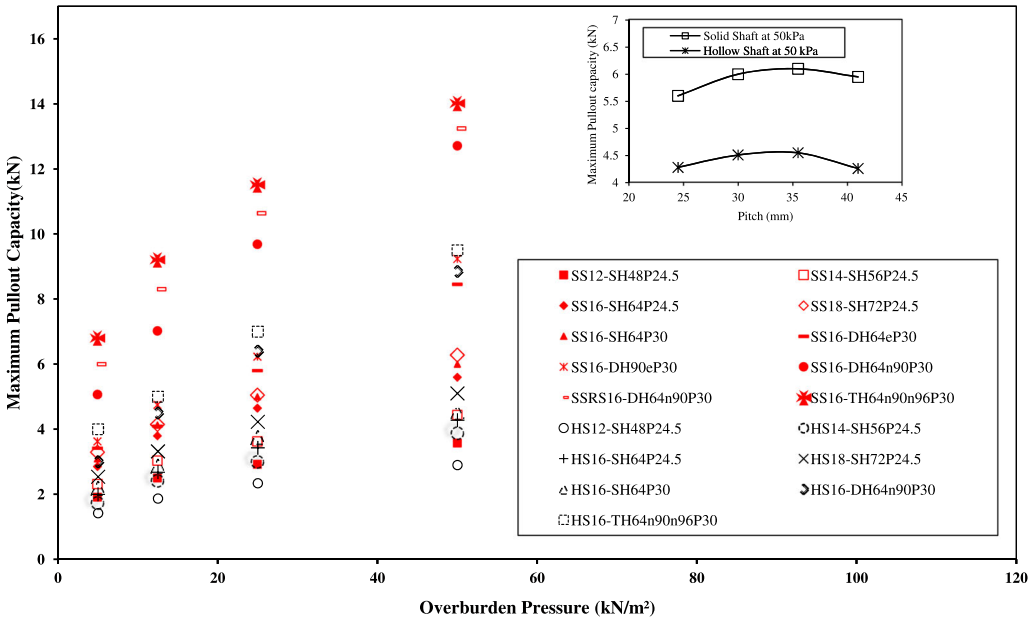

Fig. 9 Variation of maximum pullout capacity of helical nails under different overburden pressures

SH64P24.5 increases by 20.83–24.02% and 23.27–28.37%, respectively. However, the increase in average pullout force of SS18-SH72P24.5 is 9% only as compared to SS16-SH64P24.5, which is insignificant. The outcomes revealed that a small increment in pullout strength was due to large shaft and helical diameter, which creates disturbances to the adjacent soil during installation and correspondingly altering the in situ soil properties [13]. Thus, 16-mm-diameter shaft (SS16-SH64P24.5) is recommended for further alteration in helical nail configurations. Similar pattern was also observed for hollow shaft helical soil nail. Additionally, it is observed that pullout strength of SS12-SH48P24.5 and SS14-SH56P24.5 was nearly equal to the pullout strength of HS16-SH64P24.5 and HS18-SH72P24.5. So, it can be stated that there may be possibility of partial replacement of solid shaft helical nails with equivalent hollow helical shaft nails by increasing the shaft diameter by 27–34%. Thereby, cost effectiveness of helical nail manufacturing can further be enhanced.

5.3.2 Influence of helical pitch

From the literature review, it is observed that only Sharma et al. [30] have been reported on pullout behavior of helical soil nails under two different helical pitches of 23.5 and 37 mm. The authors [30] suggested that peak pullout capacity increases insignificantly with the increase in pitch. However, the study did not mention any investigation regarding the maximum allowable pitch, pitch range, or pitch effect on installation torque. Moreover, it was difficult to interpret the pullout variation beyond the predetermined pitch values of 23.5 and 37 mm. Thus, to better understand the effect of pitch on helical nail pullout, two helical nails SS16-SH64P24.5 and HS16-SH64P24.5 were chosen from the first group. The selected nails were investigated with pitch variation of 30 mm, 35.5 mm, and 41 mm, respectively. From Fig. 9, it is clear that pullout capacity increases with the increase in helical pitch. However, beyond a pitch of 35.5 mm, maximum pullout capacity is found to decrease. This can be accounted for the fact that increases in pitch initiate auguring effect in the soil. The auguring effect mainly involves crushing of soil grains during rotation and hence leading to high disturbances during installation. 'Auguring effect' is defined as the rotation of helix without the forward advancement of helical element [22]. When a helical nail is rotated during installation, the forward movement progress is slowed down or ceases which commonly causes a considerable decrease in the installation torque. The phenomenon is observed with helical plates not conforming to 'true helical shape' defined as parallel leading and trailing edges or helical plates perfectly perpendicular to the shaft. It is also observed to occur mostly when helix displaces from a less dense to more dense soil stratum. The rotation of helix with stalled advancement causes significant disturbances to the adjacent soil, and under continuous shearing, stress crushing of soil grains occurs. In the present study, the auguring effect is related during the nail installation and since pullout capacity is affected by the installation process, it has been related to the decreased pullout capacity of helical nail with large pitch of 35.5 mm. Moreover, auguring effect is also found to affect torque and pullout

capacity relationship [14]. These significant disturbances also result in reduction of ϕ, thereby corresponding to decreased pullout strength.

The reported literature also depicts same failure bulbs at the helices for different helical pitches suggesting that failure surface created about helices depends upon helix diameter rather than pitch [30]. On the contrary, the present study observed that variation in pitch influences the failure bulb development beyond 35.5 mm thus leading to a decrease in pullout capacity of the nail. For helical nails with shaft diameter of 16 mm and single helix of diameter 64 mm, maximum pullout capacity is found for pitch of 35.5 mm for solid shaft and 30 mm for hollow shaft at overburden pressure of 25 kPa. The higher pullout value of hollow shaft at a smaller pitch of 30 mm can be attributed to additional frictional resistance from soil plug formed inside the hollow shaft [7]. It can also be seen from Table 4 that percentage increase in maximum pullout capacity of helical nail SS16-SH64P35.5 in comparison with SS16-SH64P24.5 is found to be 10.14%, 10.26%, 9.46%, and 8.93% for overburden pressures of 5 kPa, 12.5 kPa, 25 kPa, and 50 kPa, respectively. Similarly, percentage increase in maximum pullout capacity for helical nail HS16-SH64P30 with respect to HS16-SH64P24.5 is 9.50%, 7.19%, 9.33%, and 5.37% for overburden pressures of 5 kPa, 12.5 kPa, 25 kPa, and 50 kPa, respectively. Thus, it can be stated that with the increase in overburden pressure and pitch from 24.5 to 35.5 mm, pullout capacity is found to increase irrespective of the shaft type, i.e., hollow or solid. Thus, a helix pitch of 30 mm is recommended for helical nail configurations for model testing. However, in full-scale practice, the recommended pitch size for helix is 76.2 mm (3 inches ± ¼ inches) [9].

5.3.3 Solid and hollow shaft with multiple helices

The pullout load–displacement responses for SS16-DH64n90P30, HS16-DH64n90P30, SSRS16-DH64n90P30, SS16-TH64n90n96P30, and HS16-TH64n90n96P30 are shown in Fig. 10. A multi-helical spacing of 3 D_h (D_h = helix diameter) based on the concept that the pressure bulbs formed around the helix do not overlap and contribute individually to pullout capacity at helix spacing of 2.5 D_h to 3.5 D_h is adopted in the present study [9]. It is observed from Table 4 that SS16-DH64n90P30 yields better pullout capacity in comparison with other solid shaft nails. The peak pullout capacity of SS16-DH64n90P30 depicts a percentage increase of 39.67%, 47.82%, 55.38%, and 37.59% in comparison with SS16-DH90eP30 under varying surcharge. Further, the average pullout capacity of SSRS16-DH64n90P30 is found to be 15% greater than SS16-DH64n90P30. The increase in pullout capacity can be accounted by additional skin friction by shaft roughness during pullout. Hence, it is suggested that shaft roughness plays an important role in enhancing the pullout capacity of helical soil nails.

The percentage increase in average pullout capacity for nail without helix (SS16) to nail with single helix (SS16-SH64P30) is approximately 409.16%. Similarly, an increase of 84.54% is found in average pullout capacity as the number of helical plates is increased from single (SS16-SH64P30) to double (SS16-DH64n90P30) helical plates. Alternatively, with the increase in helical plates from double (SS16-DH64n90P30) to triple (SS16-TH64n90n96P30), an increase of 23% in average pullout capacity is observed. Though addition of a third helix delivers an increase in pullout capacity, this increase is insignificant in comparison with percentage increase in pullout between helical nails with single helix to double helices. The reason for this insignificant pullout capacity variation can be accounted for the fact that as helices are increases from double to triple, the location of the lowermost helix may lie in zone beyond the collapse mechanism of helix underneath [11]. This would lead to only a small addition of bearing offered by the respective helix and correspondingly small increase in pullout capacity. It is evident from Fig. 9 that maximum pullout capacity varies linearly with increasing overburden pressure for different helical nails. This is indicative of the fact that pullout behavior of helical soil nail also obeys the Mohr–Coulomb failure envelop. A similar observation was also obtained by Sharma et al. [30].

The pullout resistance behavior of helical soil nails (Fig. 10) with tapered multi-helix (SS16-DH64n90P30) is better than cylindrical multi-helix (SS16-DH90eP30) at same overburden of 5 kPa. 12.5 kPa, 25 kPa, and 50 kPa, respectively. The reason can be attributed to the fact that both the helical nail configurations develop a failure surface extending along from the edges of the helix near the nail head to the helix located near the pulled end. In case of cylindrical multi-helix, a soil cylinder is formed around the nail having diameter equivalent to the helices diameter. Thus, during pullout, interface friction acts along the surface of this newly formed enlarged diameter soil tube. Alternatively, when the diameter of helices increases from nail head to nail toe (tapered multi-helix), a conical failure soil region around the nail is developed. Since the interface friction acts along the slanting surface of this conical soil region, both its horizontal and vertical components further increase the size of this conical soil surface. This results in enlarged diameter or outspread of failure soil near the pulled end of nail. Thus, large surface develops more friction against pullout and hence greater pullout capacity for tapered multi-helix nail is attained.

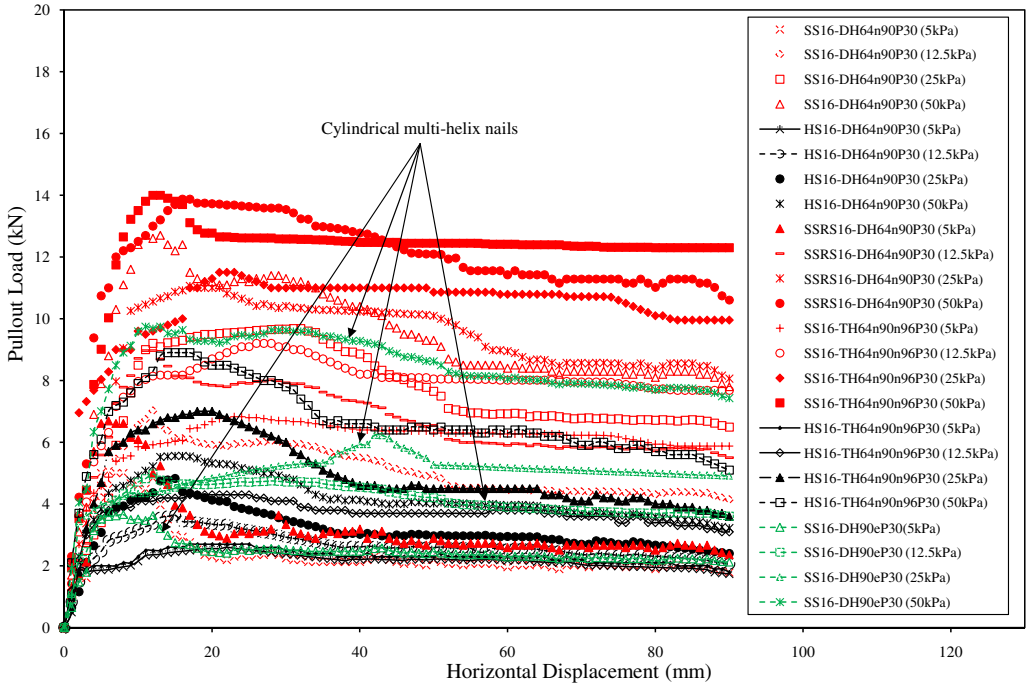

Fig. 10 Pullout load–displacement responses for different helical soil nails

5.3.4 Effect of embedment depth ratio (Z/D_h)

The pullout capacity of helical structures has been observed as a function of embedment depth in model tests [12, 14, 19, 22, 28, 30]. The embedment depth (Z) for a vertically installed helical structure corresponds to the depth of uppermost helix below the ground surface. As per the reported literature [12, 14, 19, 22, 29], failure mechanism of helical anchors is influenced by ratio of embedment depth (Z) of helical anchor to the uppermost helix diameter (D_h). It is observed that as critical embedment depth ratio $Z/D_h > 5$, transition of failure mechanism from shallow failure to deep failure occurs in case of helical anchors and piles. Based on this, transition of failure mechanism for horizontally installed helical nail is evaluated by considering the ratio of embedment depth (Z) taken as the vertical depth of outermost helix from top surface of the test tank to the diameter of outermost helix (D_h) for various adopted helical nail configurations. The variation of embedment depth ratio (Z/D_h) for helical nails is attained by the changing helix diameter only, because embedment depth (Z) is constant for all the helical nails installed horizontally [30].

In the present study, assumption of deep failure mechanism is adopted by considering $Z/D_h > 5$ for each helical soil nail configuration (Table 2). The impact of Z/D_h on helical nail pullout capacity is studied in terms of a dimensionless parameter called as Normalized Pullout Capacity or Efficiency (η). The Normalized Pullout Capacity or Efficiency (η) is defined as the ratio of pullout capacity of helical nail with different numbers of helices (Q) to pullout capacity of helical nail without helix (Q_0). It can be seen from Fig. 11 that normalized pullout capacity is found to decrease with increasing Z/D_h ratio under same overburden pressure for both solid and hollow nail shaft types. The maximum pullout efficiency is obtained for helical nail with three helices for both cases of nail shafts. Using a power regression best fit line ($R^2 = 0.865$), the efficiency (η) of a helical nail can be related to Z/D_h ratio using the relation given in Eq. (16) as:

$$\eta = \frac{125.4}{\left(Z/D_h\right)^{1.8}} \tag{16}$$

5.3.5 Soil–helical nail interaction

As reported by Jewell and Worth [15], pullout testing enables simulating restrained dilatancy and correspondingly higher bond stress as attained in fields much better than other interface tests. Thus, soil–helical nail interaction during pullout can be studied in terms of mobilized shear stress under varying overburden pressure. The pullout shear stress can be calculated using Eq. (17):

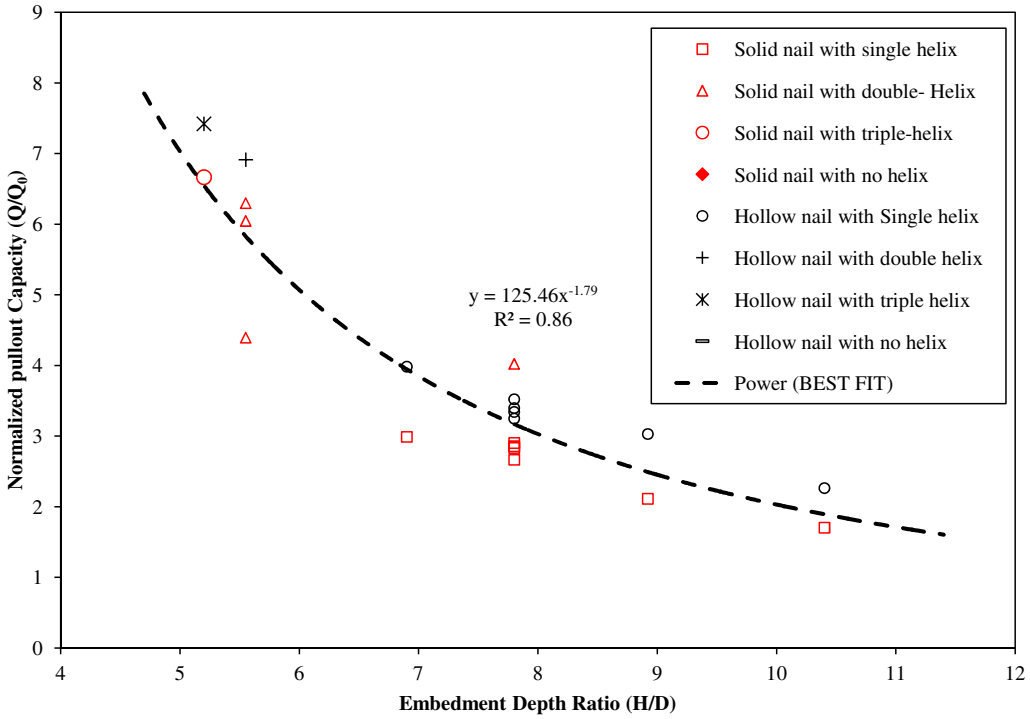

Fig. 11 Variation of normalized pullout capacity with embedment depth ratio

$$\text{Pullout shear stress} = \frac{\text{Maximum Pullout Force}(F_{\max})}{\text{Surface area of the nail } (A_s)} \tag{17}$$

where $F_{\max}$ = maximum pullout force obtained from pullout testing of helical nails, and A_s is calculated from Eq. (11). The variation of pullout shear stress with normal stress is found to follow the Mohr–Coulomb criteria (Fig. 12a). It is also observed that maximum pullout shear stress is obtained for SS16-DH64n90P30 which increases further when smooth solid shaft is replaced with rough solid shaft. However, minimum pullout shear stress is observed for SS16. In case of hollow shaft, maximum pullout shear stress is obtained for HS16-DH64n90P30 and minimum for HS16. Based on the observations, it can be extrapolated that maximum pullout shear stress will further increase with helical nail having triple helices of equivalent dimensions. Based on the Mohr–Coulomb criterion obtained, the shear strength for the soil–helical nail interface (Q_s) can be given in Eq. (18) as:

$$Q_s = c_a + \sigma_n \tan\delta \tag{18}$$

where σ_n = overburden pressure in kPa; δ = interaction friction angle in (°); and c_a = adhesion between soil and nail surface. The interaction between the soil and helical nail primarily involves frictional resistance offered by the shaft and bearing from helices. Thus, to evaluate the influence of both frictional and bearing resistances during pullout, a dimensionless parameter called interaction factor (IF) is used. The interaction factor (IF) is defined as the ratio of soil–nail interface shear strength to the applied overburden pressure and is given in Eq. (19) as:

$$\text{IF} = \frac{Q_s}{\sigma_n} \tag{19}$$

The IF values calculated for both solid and helical nails are summarized in Table 4. It can be seen from Table 4 that IF value varies from 2 to 38 for solid helical shaft. The lower boundary of IF = 2 is obtained for SS 16, whereas upper boundary of IF = 38 corresponds to SS16-TH64n90n96P30. Similarly for hollow shaft helical nails, IF is found to vary between 0.3 and 11.3. Similar to solid shaft helical nails, HS16-TH64n90n96P30 depicts a higher IF = 11.3 and lower IF = 0.3 is obtained for HS16. Moreover, higher IF values for solid shaft than hollow shafts signify a better soil–nail interaction. For helical nails of equal shaft and helix diameter with constant pitch, it is found that solid shaft renders almost 237% higher interaction than hollow shaft. It is evident from Fig. 12b that with the increase in normal stress, IF for both solid and hollow nails decreases. Likewise, under a constant normal stress, as the number of helices is increased, IF is found to increase. The influence of different nail shaft types, shaft diameter, helical pitch, and number of helices on IF values is assessed by predicting a best fit line using a power regression analysis. For solid shaft, a best fit line with

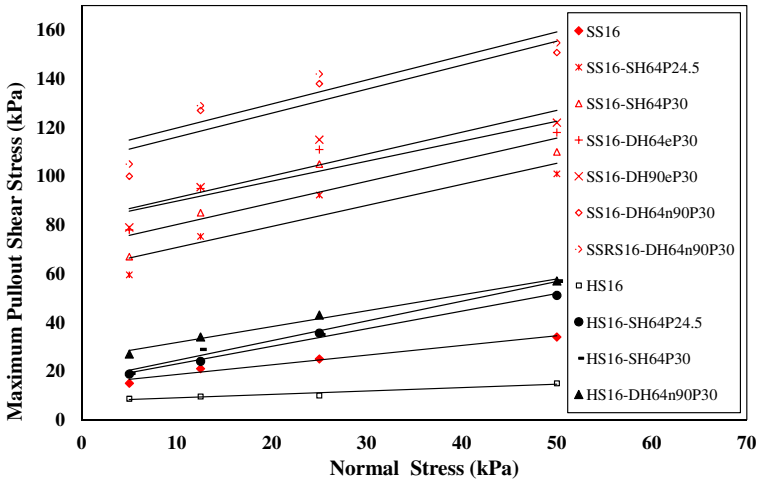

a Variations of maximum pullout shear stress and normal stress.

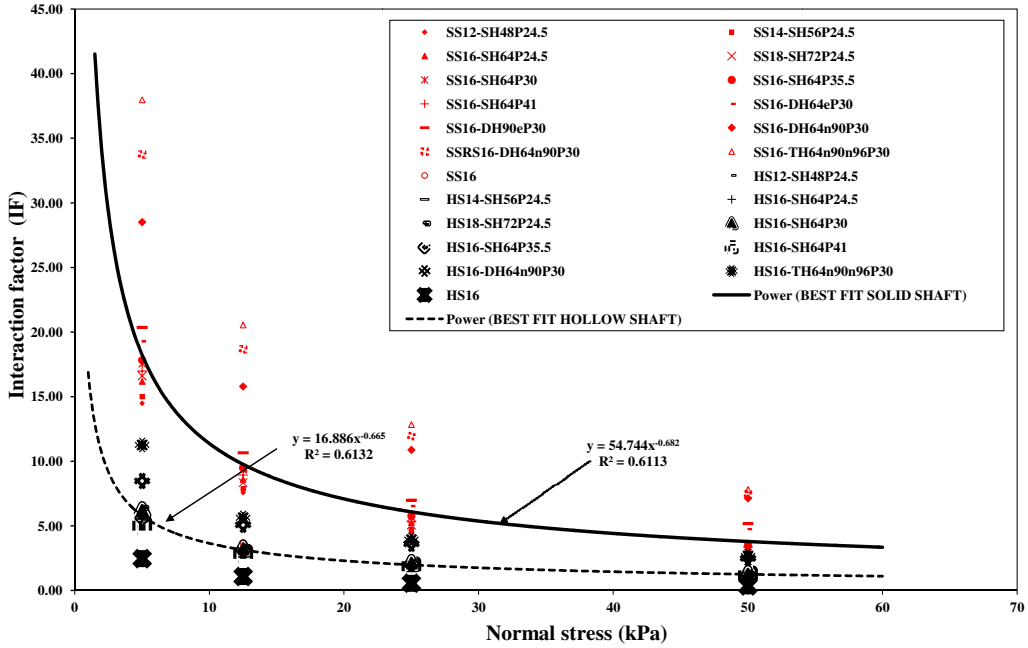

b Variation of Interaction factor with normal stress

Fig. 12 **a** Variations of maximum pullout shear stress and normal stress, **b** variation of interaction factor with normal stress

regression value of R^2 = 0.611 is attained, whereas best fit line with R^2 = 0.613 is obtained for hollow shafts. Based on the curve fitting, empirical relationship between IF values and overburden pressure (σ_n) values for different helical soil nails can be derived as given in Eq. (20):

$$\mathrm{IF} = \frac{\psi}{\sigma_n^{0.7}} \tag{20}$$

where ψ = constant having value of 55 for solid shafts helical nails and 17 for hollow shafts helical nails.

5.4 In situ stress behavior during installation and pullout

In order to examine the variation of soil stresses during installation and also during pullout of each helical soil nail, four earth pressure cells of capacity 3 MPa were placed around the installation location as shown in Fig. 13a. Two earth pressure cells were placed below the nail head, while the other two were situated below the rear end of the nail. All four earth pressure cells lie at a distance of 75 mm below the installed helical soil nail. The reported literature related to investigation of earth pressure variation during helical nail installation and pullout is very limited

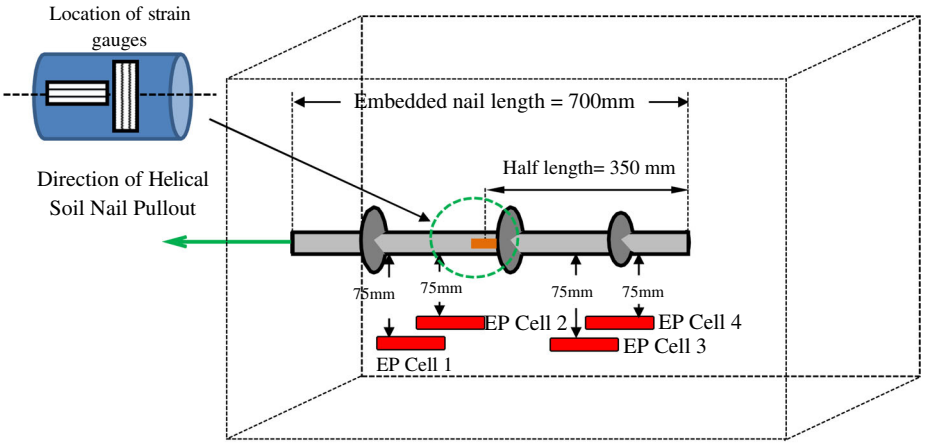

a Diagrammatic representation of the position of the earth pressure cell

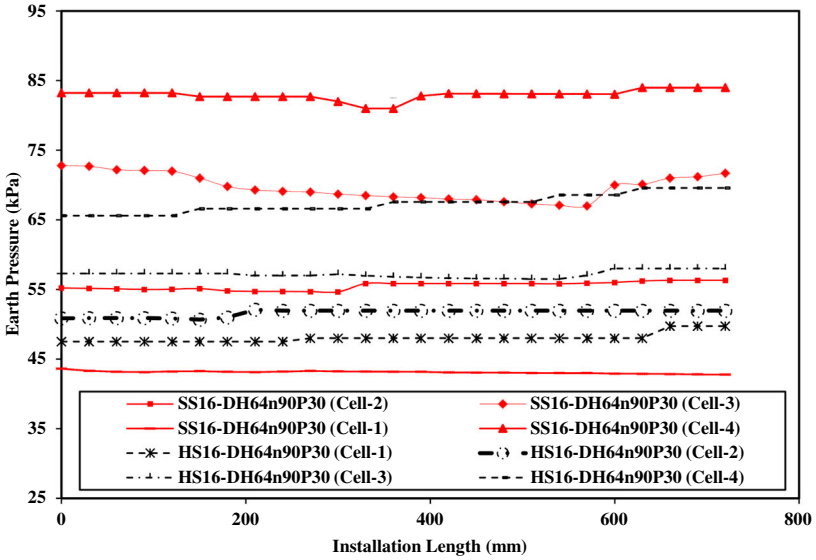

b Variation of earth pressure with Installation Length for: SS16-DH64n90P30 and HS16-DH64n90P30.

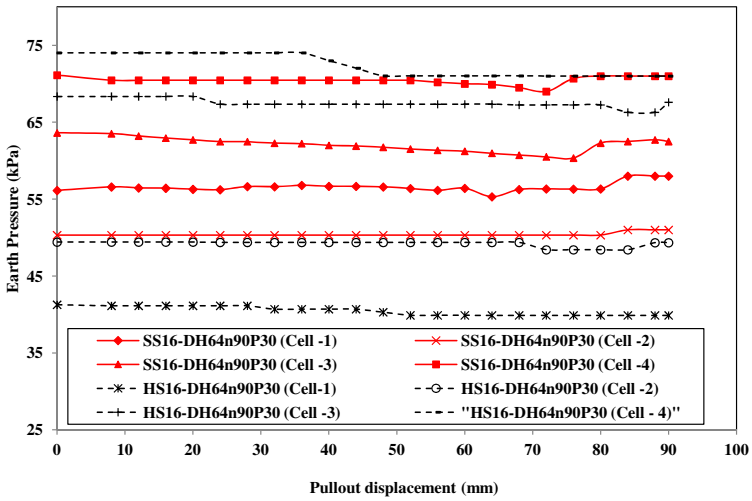

c Variation of earth pressure with pullout displacement for: SS16-DH64n90P30 and HS16-DH64n90P30.

◀**Fig. 13** **a** Diagrammatic representation of the position of the earth pressure cell, **b** variation of earth pressure with installation length for SS16-DH64n90P30 and HS16-DH64n90P30, **c** variation of earth pressure with pullout displacement for SS16-DH64n90P30 and HS16-DH64n90P30

[23, 26, 30, 34]. Moreover, the available literature is confined only to the variation of stress during installation and fails to infer any substantial information regarding the stress variation during pullout. In order to bridge this gap, Fig. 13b, c is plotted to depict the variation of earth pressure during installation and pullout of helical soil nail (SS16-DH64n90P30 and HS16-DH64n90P30) under 50 kPa, respectively. Cells 1 and 2 test the effect of installation or pullout on vertical and horizontal stresses in initial stage, whereas cells 3 and 4 measure stresses during final stage. During installation, earth pressure cells 1 and 2 record negligible variations up to installation of 330 mm of embedded nail length. However, beyond 330 mm, a small increment is noted by the pressure sensors. On the contrary, earth pressure cells 3 and 4 record small decrease in earth pressure as 200 mm of embedded nail length is installed. Between 360 and 570 mm embedded nail length earth pressure cells 3 and 4 manifest significant increment in earth pressure. This depicts that small decrease in pressure is accounted for slight disturbances caused in the soil during installation. The increment in earth pressure signifies that increase in confining pressure due to the soil densification also occurs around the nail. This increase in in situ stresses leads to an increase in pullout resistance also.

In beginning, during pullout the variations in the earth pressure at cells 1 and 2 are found nearly unchanged up to 40 mm; after that, drops in pressure have been noticed. This scenario represents that during installation of soil nail, the soil around periphery of nail slips out which creates a constant gap between nail and soil. So, when nail was pulled out, then this nail does not create any disturbance to the periphery on further pulling out soil zone suffer through soil compression. Cells 3 and 4 show a constant drop in stress and slight increment for last 10–15 mm during the pullout process for both types of nail. The drop in stress represents compression in soil due to pulling force on nail, whereas increment in stress for last 10–15 mm signifies that increase in confining pressure due to the soil densification also occurs around the nail after moving 60–70 mm of distance from its preliminary position. In addition, the earth pressures obtained from each pair of cells were different which represents that stress mobilized around helical soil nail is non-uniform.

As observed from Fig. 13c, during pullout of SS16-DH64n90P30, earth pressure decreases initially, but increases slightly as the installation progresses. This variation can be credited to the small initial displacement occurring as the helices cut through the soil and then re-densification of soil mass around the helices. Similar, trends were also observed for HS16-DH64n90P30. This indicates that hollow shaft helical nail interacts with surrounding soil on sides of the shaft, i.e., the inner side and outer side, thus leading to significant increments in confining pressure during installation. Furthermore, all test results manifest that for each helical nail configuration, minimal stress variations have been observed, whereas for conventional nails large in situ stress variations are reported due to boring and subsequent grouting [33]. Hence, this reveals that helical soil nails generate significantly less disturbances in in situ soil during installation as compared to grouted soil nails. Moreover, this privilege is offered without any compromises in the pullout capacities.

5.5 Development of axial strains and settlement of ground surface

The axial strains were measured using four strain gauges, located at the 350 mm from the nail head (i.e., embedded length (700 mm)/2) on opposite sides of the nail shaft. Two strain gauges were placed along the nail axis, while the other two are perpendicular to the nail axis (Fig. 13a) [20]. To assure connections remain intact during installation and pullout, strain gauges were protected using adhesive tapes. The strain gauge wiring was connected to a terminal pad to increase the safety of connection. Strains are normally taken into account for long-term performance monitoring of a soil-nailed structure [8]. As evident from Fig. 14a, hollow shaft helical soil nails develop more axial strains during pullout as compared to solid shaft helical nails. It can also be noted that development of axial strains is also affected by the number of helical plates attached to the shaft. The strains generated in HS12-SH48P24.5 are more than that in HS16-TH64n90n96P30. With the latter depicting the minimum strain values with pullout slip, it can be deduced that helical nail with hollow shaft and single helix shows maximum axial strain generation, whereas with triple helices, strain generation falls off to the lowest. A hollow helical shaft nail with double helices depicts an intermediate effect for axial strain generation. The strain generation behavior can also be a reason for lower pullout resistance offered by HS12-SH48P24.5 in comparison with maximum pullout resistance obtained for HS16-TH64n90n96P30. In case of solid shaft helical nails, it can be noted that maximum strain generation is observed for SS12-SH48P24.5, which is similar to hollow nails. As the pullout slip increases, strains generated in both double and triple helices become almost same. Additionally, in case of rough solid shaft, lower strain values than helical

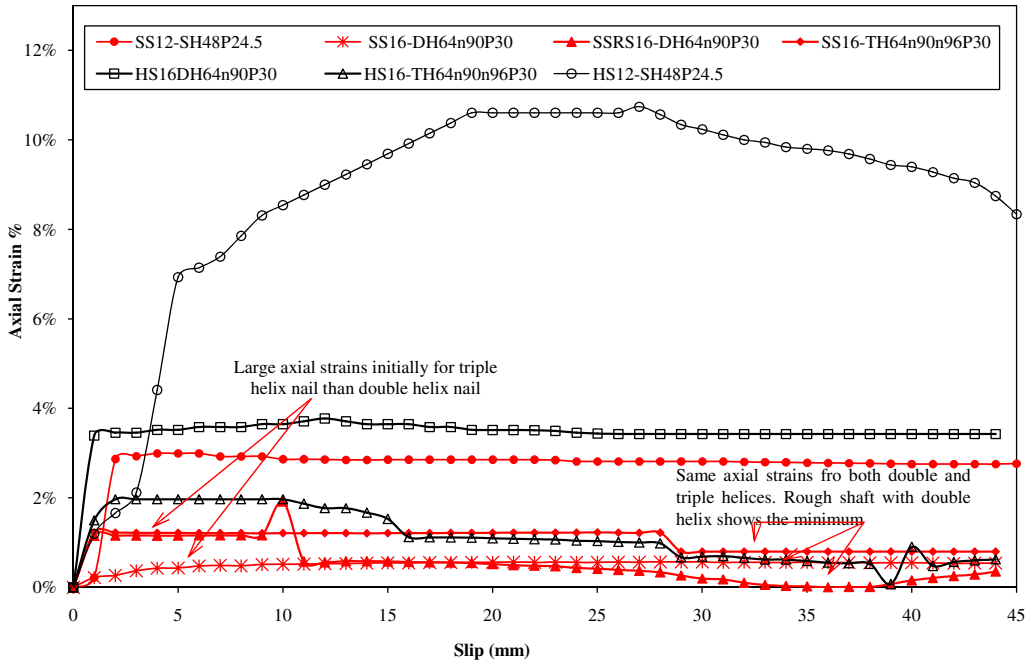

a Axial strain % versus horizontal displacement for different helical soil nails

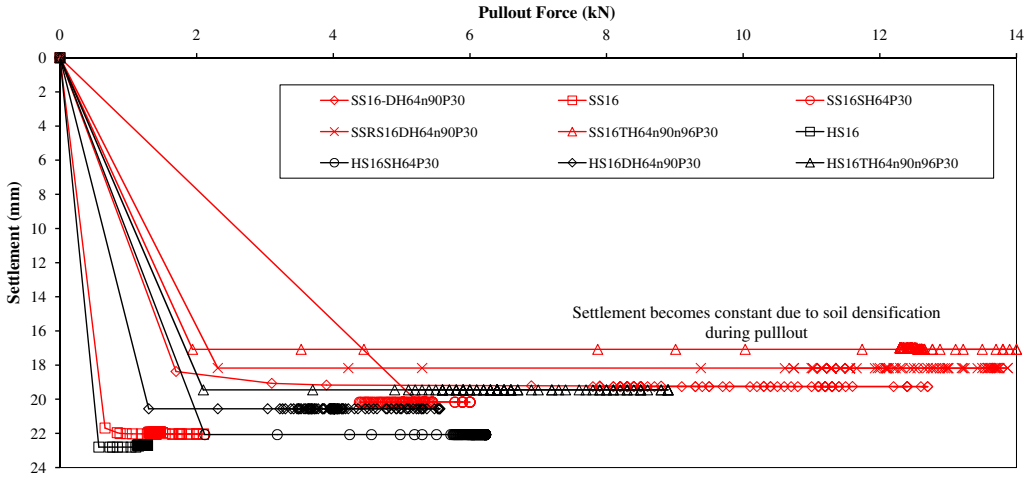

b Variation of Pullout force with settlement under overburden pressure of 50kPa

Fig. 14 **a** Axial strain % versus horizontal displacement for different helical soil nails, **b** variation of pullout force with settlement under overburden pressure of 50 kPa

nail with triple helices are still persistent for large pullout slip. The variation of these strains with pullout slip also satisfies the condition of attaining maximum pullout for solid rough shaft (SSRS16-DH64n90nP30) in comparison with smooth shaft. Moreover, pullout capacity of SS16-DH64n90nP30 is found approximately equal to that of SS16-TH64n90n96P30.

Further, it is observed that top plate on the soil tank was found to settle during the pullout of helical nails. It was observed that the amount of settlement during pullout of hollow nail shafts was greater than solid shafts. It can be seen from Fig. 14b that for identical configuration of helical nails, greater vertical settlement of top plate with pullout of hollow nails is observed as compared to pullout of solid nails. As hollow shaft 'HS16' and solid shaft 'SS16' nail are installed, the nail head displaces soil volume corresponding to half of the shaft diameter [14]. The soil displacement during solid shaft installation is greater as compared to hollow shaft leading to higher soil densification around the solid shafts. Alternatively, during installation of hollow shafts, outward soil displacement is accompanied by fraction of soil moving into the hollow

tubular shaft. Due to this, soil displacement achieved is small and consequently less soil densification around hollow shafts is attained. Therefore, as solid shaft 'SS16' is pulled out, the densified soil provides greater bearing against applied load and undergoes less settlement as compared to HS 16 nail. From Fig. 14b, it is also evident that settlement value reduces with the increase in number of helices for both hollow and solid shaft nails. This settlement behavior of nails with helical plates can be attributed to the fact that soil ahead of the helical plates displaces from its equilibrium condition during pullout, thereby creating a momentary void between the nail and soil. As the helix shifts from one position to other, the gap is filled up by the preceding soil displaced from the following helix. Thus, rapid filling of void and consequently smaller settlement is achieved for nails with triple helices in comparison with single and double helix.

6 Conclusions

The present study evaluates the experimental results on single and multi-helical soil nails with smooth solid, smooth hollow, and rough solid shafts under variation of parameters such as installation torque, pullout behavior, pitch variation, embedment ratios, soil–nail interaction, in situ stresses, axial strain variation, and ground settlement. Based on the outcomes achieved, the following conclusions are drawn:

1. The installation torque to pullout capacity of helical soil nails can also be correlated using an empirical factor K_t as for the case of helical anchors and helical piles. However, K_t for helical soil nails with solid shaft ranges from 19 to 61 m^{-1} and 23 to 58 m^{-1} for helical soil nails with hollow shafts. K_t decreases with the increase in embedded helical nail area and exponential of nail shaft diameter ($d^{0.54}$). During helical nail installation, strain-softening phenomenon is observed for both cases of hollow and solid shafts.
2. The installation torque increases with shaft and helix diameter, number of helices, and overburden pressure from 5 to 12.5 kPa and falls off gradually till 50 kPa. The solid shaft nails depict higher installation torque in comparison with hollow shaft nails for all D_h/d and D_h/P ratio. Thus, it can be concluded that helical soil nails having solid shaft require greater installation torque for all variations of shaft diameter, helix diameter, pitch, and number of helices.
3. The variation of maximum pullout under increasing overburden pressure follows Mohr–Coulomb failure criteria. Similar results were also obtained from direct shear test for different interfaces. The failure envelops for soil–rough surface solid shaft interface depict maximum interface friction angle in comparison with soil–smooth hollow shaft interface and soil–smooth solid shafts interface. Higher interaction factor (IF) values in the range of 2–38 are obtained for solid shafts as compared to hollow shafts with IF values in the range of 0.3–11.3. The IF values increase as the number of helices increases along the nail shaft for both solid and hollow nails. In addition, the nail with rough shaft contributes significantly to IF and pullout capacity.
4. Significant increment in the pullout capacity is obtained with the increase in number of helical plates from single to multi-helix. The maximum pullout capacity is attained for a pitch of 30 mm and is thus recommended for model testing purposes. However, addition of a third helix brings only a small increment in pullout capacity under increasing overburden pressure for both hollow and solid shafts. The normalized pullout capacity is found to decrease with increasing Z/D_h under same overburden pressure. However, beyond $Z/D_h = 10.4$, pullout efficiency of both multi-helix and helical nails without helix is same.
5. The variation of in situ stresses developed during installation and pullout of multi-helix nail is lower than helical nail without helix or conventional soil nails. Thus, it can be concluded that helical soil nails exhibit significantly lesser disturbances during installation and pullout in comparison with conventional soil nails.
6. The axial strain for smaller diameter shafts (both solid and hollow shafts) is more than for equivalent large diameter shafts. Helical nail with more number of helical plates depicts lower axial strains, higher pullout, and consequently higher installation torque as compared to helical nails with less helical plates. The settlement of ground surface reduces as the number of helices increases.

Acknowledgment The authors are extremely grateful to both the reviewers for investing their valuable time in enhancing the scientific merit and overall presentation of the manuscript. The reviewers' suggestions and knowledge sharing have significantly improved the final version of the presented work. The authors also acknowledge the support from Er. Manoj Sharma, Head of Maintenance Department, JUIT, in fabrication of the pullout setup. The authors are also thankful to Mr. Jaswinder Deswal and Mr. Rajesh Sahu for providing assistance during laboratory testing.

References

1. Aziz E, Stephens T (2013) Cost and schedule savings from directly-driven soil nail and innovative fascia systems. GeoCongress 2013:1704–1718. https://doi.org/10.1061/9780784412787.171

2. Bagheri F, El Naggar (2015) Effects of installation disturbance on behavior of multi-helix piles in structured clays. DFI J—J Deep Found Inst 9(2):80–91. https://doi.org/10.1179/1937525515Y.0000000008
3. Bowen G (2009) a static based theory for the capacity to torque factor for helical piers in compression. In: Proceedings of helical foundations and tie-backs seminar, deep foundation institute, University of Alberta, Canada, June 2009
4. Chu LM, Yin JHA (2005) Laboratory device to test the pull out behavior of soil nails. ASTM Geotech Test J 28(5):499–513
5. Chu LM, Yin JH (2005) Comparison of interface shear strength of soil nails measured by both direct shear box tests and pullout tests. J Geotechn Geo-environ Eng 131:1097–1107
6. Emam ME, Attom M, Khan Z (2012) Numerical prediction of plane strain properties of sandy soil from direct shear test. Int J Geotech Eng 6(1):79–90. https://doi.org/10.3328/ijge.2012.06.01.79-90
7. Han Fei, Ganju Eshan, Salgado Rodrigo, Prezzi Monica (2019) Comparison of the load response of closed-ended and open-ended pipe piles driven in gravelly sand. Acta Geotech. https://doi.org/10.1007/s11440-019-00863-1
8. FHWA (2015) Geotechnical engineering circular No. 7: Soil nail walls—reference manual. FHWA, Washington, D.C. Rep. No. FHWA-NHI-14-007
9. FSI (2014) Technical manual: helical piles and anchors, hydraulically driven push piers, polyurethane injection & supplemental support systems, 2nd edn. Foundation Support Works, Omaha, pp 33–39
10. Ghaly A, Hanna A, Hanna M (1991) Installation torque of screw anchors in sand. Soils Found 31(2):77–92. https://doi.org/10.3208/sandf1972.31.2_77
11. Hao D, Wang D, Loughlin C, Gaudin C (2018) Tensile monotonic capacity of helical anchors in sand: interaction between helices. Can Geotech J. https://doi.org/10.1139/cgj-2018-0202
12. Hoyt RM, Clemence SP (1989) Uplift capacity of helical anchors in soil. In: Proceedings 12th international conference on soil Mech. and Found. Eng., Brasil, vol 2, pp. 1019–1022
13. Hubbell Power Systems Inc (2015) Screw nailing retention earth structures, design manual, Chance USA
14. Hubbell Power Systems, Inc. (2018) HUBBELL Technical Design Manual Edition 4. Chance Atlas
15. Jewell RA, Wroth CP (1987) Direct shear tests on reinforced sand. Géotechnique 37(1):53–68. https://doi.org/10.1680/geot.1987.37.1.53
16. Junaideen SM, Tham LG, Law KT, Lee CF, Yue ZQ (2004) Laboratory study of soil–nail interaction in loose, completely decomposed granite. Can Geotech J 41(2):274–286. https://doi.org/10.1139/t03-094
17. Lindsay FM, Mickovski SB, Smith MJ (2015) Testing of self-drilled hollow bar soil nails. In: Geotechnical engineering for infrastructure and development, pp 2969–2974
18. Liu J, Liu M, Zhu Z (2012) Sand deformation around an uplift plate anchor. J Geotechn Geo-Environ Eng 138(6):728–737
19. Merifield RS, Sloan SW (2006) The ultimate pullout capacity of anchors in frictional soils. Can Geotech J 43(8):852–868. https://doi.org/10.1139/t06-052
20. Omega.co.uk (Strain gages manual). Positioning strain gages to monitor bending, axial, shear, and torsional loads: a guide to installation (E56). http://www.personal.umich.edu/~bkerkez/courses/cee575/Handouts/2strainpositioning.pdf. Accessed 2019
21. Pradhan B, Tham LG, Yue ZQ, Junaideen SM, Lee CF (2006) Soil-nail pullout interaction in loose fill materials. Int J Geomech 6(4):238–247. https://doi.org/10.1061/(ASCE)1532-3641(2006)6:4(238)
22. Perko HA (2009) Helical piles: a practical guide to design and installation. Wiley, Hoboken
23. Rawat S, Gupta AK (2017) Testing and modeling of screw nailed soil slopes. Indian Geotech J 48(1):52–71. https://doi.org/10.1007/s40098-017-0229-7
24. Rawat S, Gupta AK (2017) Numerical modelling of pullout of helical soil nail. J Rock Mech Geotechn Eng 9(4):648–658. https://doi.org/10.1016/j.jrmge.2017.01.007
25. Rawat S, Gupta AK, Kumar A (2017) Pullout of soil nail with circular discs: a three-dimensional finite element analysis. J Rock Mech Geotechn Eng 9:967–980. https://doi.org/10.1016/j.jrmge.2017.05.003
26. Rawat S (2017) Testing and Modeling of soil–nailed slopes. Dissertation, Jaypee University of Information Technology, Waknaghat, Solan, Himachal Pradesh, India
27. Rotte VM, Viswanadham BVS (2013) Influence of nail inclination and facing material type on soil-nailed slopes. Proc ICE-Ground Improve 166(2):86–107. https://doi.org/10.1680/grim.11.00026
28. Sakr M (2015) Relationship between installation torque and axial capacities of helical piles in cohesionless soils. Can Geotech J 52(6):747–759. https://doi.org/10.1139/cgj-2013-0395
29. Schiavon JA, Tsuha C, Thorel L (2016) Scale effect in centrifuge tests of helical anchors in sand. Int J Phys Modell Geotechn 16(4):185–196. https://doi.org/10.1680/jphmg.15.00047
30. Sharma M, Samanta M, Sarkar, S (2017) A laboratory study on pullout capacity of helical soil nail in cohesionless soil. Can Geotech J 54(10):1482–1495. https://doi.org/10.1139/cgj-2016-0243
31. Sharma P, Rawat S, Gupta AK (2018) Study and remedy of kotropi landslide in Himachal Pradesh, India. Indian Geotechn J 48(4):1–17. https://doi.org/10.1007/s40098-018-0343-1
32. Su LJ, Chan TCF, Shiu YK, Cheung T, Yin JH (2007) Influence of degree of saturation on soil nail pullout resistance in compacted completely decomposed granite fill. Can Geotech J 44(11):1314–1328. https://doi.org/10.1139/T07-056
33. Su LJ, Chan TCF, Yin JH, Shiu HYK, Chiu SL (2008) Influence of overburden pressure on soil nails pull-out resistance in a compacted fill. J Geotechn Geoenviron Eng 134(9):1339–1347. https://doi.org/10.1061/(ASCE)1090-0241(2008)134:9(1339)
34. Tokhi H (2016) A study of new screw soil nail. Dissertation, RMIT University, Melbourne
35. Tsuha C, Aoki N (2010) Relationship between installation torque and uplift capacity of deep helical piles in sand. Can Geotech J 47(6):635–647. https://doi.org/10.1139/t09-128
36. Wang Z, Richwien W (2002) A study of soil-reinforcement interface friction. J Geotechn Geoenviron Eng 128(1):92–94. https://doi.org/10.1061/(asce)1090-0241(2002)128:1(92)
37. Yin JH, Zhou WH (2009) Influence of grouting pressure and overburden stress on the interface resistance of a soil nail. J Geotech Geoenviron Eng 135(9):1198–1208. https://doi.org/10.1061/ascegt.1943-5606.0000045
38. Zhang LL, Zhang LM (2009) Tang WH (2009) Uncertainty of field pullout resistance of soil nails. J Geotechn Geoenviron Eng 135(7):966–972
39. Zhou W (2008) Experimental and theoretical study on pullout resistance of grouted soil nails. Dissertation, The Hong Kong Polytechnic University